

# Electrocatalytic oxidation of glucose using metal oxide nanoparticle-based electrodes

Mahmoud M. Saleh<sup>1,2,#</sup>, O. A. Hazazi<sup>3</sup> and Mohamed I. Awad<sup>1,3,\*</sup>

<sup>1</sup>Department of Chemistry, Faculty of Science, Cairo University, Giza, Egypt.

<sup>2</sup>Chemistry Department, College of Science, King Faisal University, Al-Hassa, Saudi Arabia;

<sup>3</sup>Chemistry Department, Faculty of Applied Sciences, Umm Al-Qura University, Makkah Al Mukarramah, 13401, Saudi Arabia.

## ABSTRACT

The research on finding new and efficient catalysts for important electrochemical reactions such as glucose oxidation has never ceased since it is of core interest in the development of important devices such as fuel cells and biosensors. Electrocatalytic oxidation of glucose is an important topic both from the academic and technological points of view. While many researchers have treated the issue from the analytical chemistry point of view, others have studied this reaction (oxidation of glucose) as a half-cell reaction in biofuel cells. Precious metals such as platinum, gold and palladium are in many cases unavoidable candidates for glucose oxidation. However, these noble metals, in addition to their high cost, suffer from high susceptibility to poisoning by oxidation products. Thus scientists have been offering solutions to replace such costly noble metals with low-cost metals and metal oxides such as NiO, CuO and MnO<sub>2</sub>. In recent years metal oxide nanoparticle-based electrodes have been used for glucose oxidation in alkaline solutions. On one hand, they meet the necessities of the development of biofuel cells and on the other, they aid the development of biosensors directed towards glucose sensing in blood and in food industry. In this context, this review is intended to shed some light on the

electrocatalytic oxidation of glucose using metal oxide (both single and binary) nanoparticle-based electrodes. Special attention is given to the methods of synthesis of such nanoparticles, surface techniques for their characterization and applications to glucose oxidation in alkaline solutions.

**KEYWORDS:** binary, nanoparticles, glucose, oxide, electrocatalyst

## 1. Introduction

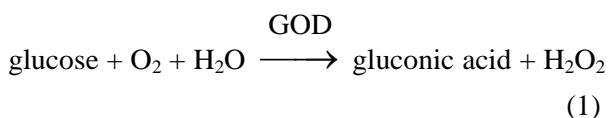
Glucose electrooxidation is of prime importance for the diagnosis of diabetes mellitus, for food preparation processes and for the development of biofuel cells [1-5]. Glucose electroensing is achieved either through enzyme-based or enzymeless methods. When using enzyme-based methods, it can be carried out in the presence of either a free enzyme or an immobilized one. Enzyme-based electroensing is characterized by its high selectivity and it is the widely accepted approach since 1967 [6]. Most of enzymatic sensors are operated in the presence of either mediators or catalysts which are used to carry out the effective electrical contact of the enzyme active center with electrodes [7, 8]. The enzyme is utilized in the conversion of the analyte into electroactive species. This method of analysis is constrained by some restrictions such as the prerequisite of a biocompatible matrix as support, limited stability and oxygen deficit under low oxygen pressure, in addition to the difficult immobilization of the enzyme [9, 10].

---

\*Corresponding author: mawad70@yahoo.com

#mahmoudsaleh90@yahoo.com

Since their invention by Clark and Lyons in 1962, enzyme-based electrodes have been further developed and modified during the last few decades to meet the requirements of use as glucose enzymatic biosensors [11]. In general, glucose oxidase (GOD)-based method has been the most widely used. Analysis of glucose is based on reaction 1 (see below) where GOD can convert glucose to gluconic acid, liberating hydrogen peroxide ( $\text{H}_2\text{O}_2$ ). Thus the glucose was sensed either by measuring the consumption of oxygen or the liberated  $\text{H}_2\text{O}_2$  [12].



Enzyme-based electrodes have been fabricated either by physical entrapping of enzyme molecules within conducting polymer films or by covalent bonding of the enzyme with the functional group of an underlying matrix. In the former modification, the enzyme is entrapped deeply into the conducting matrix and hence it contributes little to the sensing ability [13-23]. Immobilized enzymes have many operational advantages over free enzymes such as the possibility of continuous operation, modulation of catalytic properties, lower cost of operation, reusability, good stability and wider working concentration range of analytes [24-26]. However, the lifetime of the enzyme-based sensors is limited [27, 28]. Therefore, several other procedures have been developed to overcome the above problem. They include immobilization of the enzymes onto metallic substrates through a thin film of self-assembled monolayer and conducting polymers [29-33]. Recently, nanostructured materials have been used as substrates or platforms for immobilizing enzymes because of their favorable intriguing properties such as large surface-to-volume ratio and high catalytic and surface reaction activity. However, most of these nanomaterials require cross-linking reagents or Nafion films to prevent enzyme leaching from electrode surface [34]. Hence, this calls for new methods that can overcome the above-mentioned obstacles.

Enzymeless glucose sensors have found their use as a promising alternative for enzyme-based analysis [35]. Considerable efforts have been focused in this direction in the last decade. Electrocatalysts

designed for sensing or electrocatalysis of glucose oxidation usually use a single or bimetallic catalyst fabricated from metal and/or metal oxide nanoparticle-based electrodes.

Noble metals, as an important category of transition metals, have been extensively used for the purpose of enzymeless electroanalysis of glucose owing to their unique electrocatalytic properties, biocompatibility, fascinating surface structure, good electrical and mechanical properties, good electrocatalytic activity, strong stability and limited aggregation, and high performance [36, 37].

Gold is an important candidate for electrocatalysis of glucose oxidation as it presents high selectivity as well as sensitivity. The high selectivity is attributed to the electro-oxidation of glucose at Au electrodes at relatively high negative potential both in neutral and alkaline media [38]. However, the electro-oxidation of glucose at Au electrodes has been faced with two main problems. First is the interference from ascorbic acid (AA), and the other one is the deactivation of the electrode activity by  $\text{Cl}^-$  ions [39, 40]. Chlorides, getting adsorbed at gold active sites inhibit the glucose oxidative-adsorption, which is the first and key step of the failure of the oxidation mechanism [41]. Toghil and Compton reported this problem earlier in 2010 [35]. After that, a number of approaches have been reported including that of gold-modified electrodes [42-46]. Au electrode surfaces with porous structures have been successfully used to eliminate interference from AA [47-52].

Several strategies have been explored for the preparation of nanostructured Au-modified electrodes in recent years. Nanoporous gold electrodes have been prepared mainly by de-alloying [53, 54] and anodization [55-59]. Pd coated nanoporous gold films [60] have been shown to improve the catalytic activity and enhance the stability for glucose oxidation [61, 62]. Pd nanoparticles have been dispersed on a variety of substrates such as indium tin oxide, carbon nanotubes [63, 64], epoxy-silver [65], graphene nanohybrids [66], boron-doped diamond [67], and polymers [68-70].

Cu-modified electrodes, characterized by their low cost and ease of fabrication, have received

considerable attention due to their electrocatalytic activity for glucose oxidation [71]. The effect of the underlying substrate on the electrocatalytic properties of copper-modified electrodes has also been reported [72, 73]. Recently, combining copper based materials with carbon nanotubes for glucose detection has been widely investigated. This has been achieved by sputtering cupric oxide on multi-walled carbon nanotubes (MWCNTs) [74, 75], electrodepositing copper nanocubes onto vertically-well-aligned MWCNTs [76], electrochemical deposition of copper oxide nanoparticles on horizontally-aligned single-walled carbon nanotubes (SWCNTs) [77], seed-mediated growth synthesis of copper nanoparticles on carbon nanotubes (CNTs) [78], copper oxide nanoleaves decorated CNTs [79] and nanospindle-like cuprous oxide/straight CNT nanohybrids [80].

Ni-based nanomaterials have exhibited remarkable catalytic oxidation for glucose originating from the redox couple of Ni(II)/Ni(III) formed on the electrode surface in alkaline medium [81, 82]. Most of the Ni-based glucose sensors were fabricated by modifying traditional electrodes with Ni-based nanomaterials such as dispersing Ni nanoparticles in disordered graphite-like carbon [83], doping carbon paste electrode with nano-NiO powder [84] and mixing powdered nanoscale nickel hydroxide with graphite powder in ionic liquid [85].

Platinum was the first discovered material that demonstrated electrocatalytic activity for glucose oxidation [86]. However, glucose sensors using Pt electrode suffer from poisoning by adsorbed intermediates and interfering species in addition to the oxidation of glucose at relatively higher potentials. This results in low sensitivity and poor selectivity [87-91]. This problem had been partially resolved by using another metal (e.g., Ni and Co) as a co-catalyst. Beside reducing Pt loading, the metal offers better tolerance to the poisoning of Pt by acting as a sacrificial active site on which the oxidation products are preferentially adsorbed [92, 93].

Pt-based electrocatalysts, PtM (M = Ru, Pd, Au, Ni, Ag, Bi, Pb) are currently drawing much attention because of their unique catalytic behavior compared to that offered by single-metal catalysts. They provide rapid response, good stability, and high

catalytic efficiency [94-113]. Also, Au-based bimetallic catalysts, AuM (M = Pt, Pd, Ag) have been reported [105, 106]. Other bimetallic catalysts have been reported albeit not extensively as those of the combination of either Pt or Au with other metals [107].

Recently, large numbers of transition metal oxides, including both bulk and nanostructures-based ones, such as NiO<sub>x</sub>, FeOOH, CuO, MnO<sub>2</sub>, RuO<sub>2</sub>, CuO<sub>x</sub>, ZnO and Co<sub>3</sub>O<sub>4</sub> have been reported for use as non-enzymatic electrocatalysts for glucose oxidation as an alternative for costly noble metals [114-124]. Among these oxides, NiO<sub>x</sub> and CuO<sub>x</sub> received substantial attention because of their low cost and environmental safety [125-140].

Copper oxides (CuO, Cu<sub>2</sub>O), as an important class of p-type semiconductor metal oxides, have attracted considerable attention for use in enzyme-free glucose sensors due to their high electrocatalytic activity resulting from the multi-electron oxidation mediated by surface metal oxide layers [141-148]. Since the catalytic activities of the nanoscale materials are closely related to their shapes, many efforts have been made on amperometric determination of glucose using nanostructured copper oxides with various morphologies including platelets [142], fibers [144], spindles [144], particles [144], wires [144, 147], rods [145], flowers [145, 146], urchins [147], cubes [118] and spheres [148].

Among many possible electrocatalytic materials, those with the nickel redox couple Ni(II)/Ni(III) are of particular interest and have been the subject of much investigation. A survey of the literature shows that various studies have been devoted to investigations of the electrochemistry of a nickel hydroxide/oxyhydroxide couple [149-152]. Nickel oxyhydroxide strongly adsorbs some of the organic substances and has high electrocatalytic efficiency for the oxidation of organic molecules via cyclic mediation electron-transfer processes in alkaline solutions.

## 2. Glucose oxidation on NiO<sub>x</sub> and MnO<sub>y</sub>/NiO<sub>x</sub>

In this part, our recently published work on electrocatalytic glucose oxidation at single and binary catalyst-modified glassy carbon electrodes is reviewed [153-157]. In single catalyst-modified electrodes, NiO<sub>x</sub>-nanoparticles were electrodeposited

on either bare or anodically-oxidized glassy carbon electrodes. In binary catalysts,  $\text{NiO}_x$ - and  $\text{MnO}_y$ -modified glassy carbon electrodes were used for the electrocatalytic oxidation of glucose in alkaline solutions. Although binary catalysts composed of nickel with either manganese oxides or copper oxides have been documented [152], both metals were deposited simultaneously from a mixture of their ions. In our work, the bicatalyst ( $\text{NiO}_x$  and  $\text{MnO}_y$ ) was electrodeposited in a well-ordered sequence. The order was found to have significant impacts on the electrocatalytic properties of the binary catalysts on glucose oxidation.

## 2.1. Binary catalysts

This section presents the electrocatalytic activity of a new catalyst composed of nickel and manganese binary oxides, prepared by sequential electrodeposition, for glucose electrooxidation in an alkaline solution.

### 2.1.1. Electrode modification

Glassy carbon electrode (GCE) modification with  $\text{NiO}_x$  and  $\text{MnO}_y$  were achieved in two sequential steps. First was the potentiostatic deposition of metallic nickel on the GCE from an aqueous solution of 0.1 M acetate buffer solution (pH = 4.0) containing 1 mM  $\text{Ni}(\text{NO}_3)_2 \cdot 6\text{H}_2\text{O}$  by applying a constant-potential electrolysis at -1 V (Ag/AgCl/KCl) for different time durations. Next, the deposited Ni was passivated in 0.1 M phosphate buffer solution (PBS, pH = 7) by cycling the potential between -0.5 and 1 V for 10 cycles at a scan rate of 200 mV/s [154]. Then the modification with  $\text{MnO}_y$  was achieved by cycling the potential from 0 to 0.4 in 0.1 M  $\text{Na}_2\text{SO}_4$  containing 0.1 M  $\text{Mn}(\text{CH}_3\text{COO})_2 \cdot 5\text{H}_2\text{O}$  for 60 cycles, then activation by potential cycling for 5 cycles in 0.5 M NaOH solution in the potential range -0.2 to 0.6 V [154]. The sequence of the deposition of the two catalysts, i.e.,  $\text{NiO}_x$  deposited first and then  $\text{MnO}_y$  or vice versa, was achieved by keeping the number of  $\text{MnO}_y$  cycles constant at 60 cycles and changing the deposition time of  $\text{NiO}_x$ .

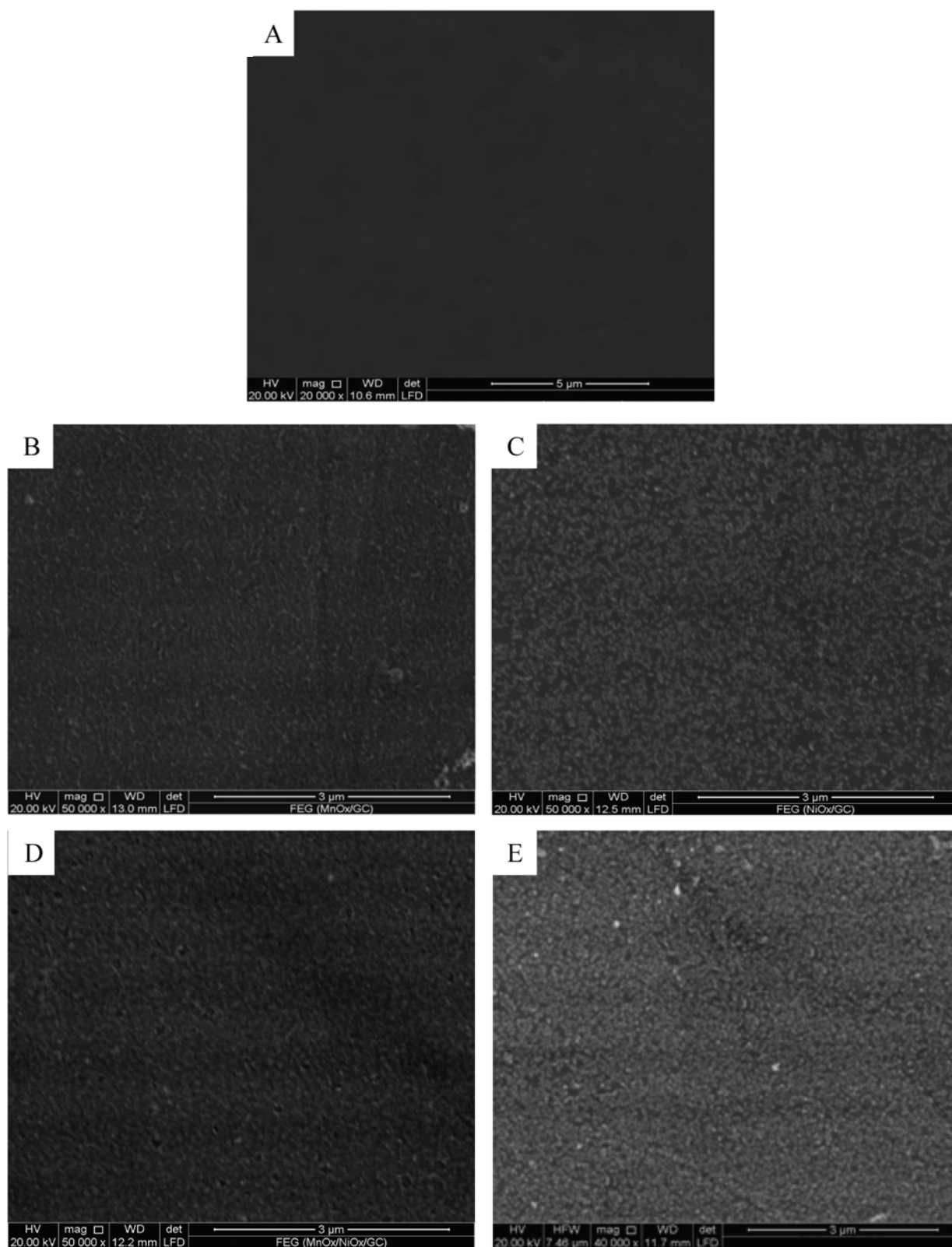
### 2.1.2. Morphological and electrochemical characterizations

Fig. 1 shows scanning electron microscopy (SEM) images taken for bare glassy carbon electrode (GCE) (A),  $\text{MnO}_y/\text{GC}$  (B),  $\text{NiO}_x/\text{GC}$  (C),

$\text{MnO}_y/\text{NiO}_x/\text{GC}$  (D), and  $\text{NiO}_x/\text{MnO}_y/\text{GC}$  (E) electrodes. In image (A), the GC substrate is featureless whereas  $\text{MnO}_y$  is deposited exhibiting a porous nanorod-texture (image B) [155]. The  $\text{NiO}_x$  nanoparticles are uniformly deposited on the GC substrate with an average particle size of about 90-100 nm (image C). In image (D) ( $\text{MnO}_y/\text{NiO}_x/\text{GC}$  sample,  $\text{NiO}_x$  is deposited first), the microstructure is significantly different compared with the image of direct deposition of  $\text{MnO}_y$  on bare GC (image B), and it appears as a combined feature of images (B) and (C), where particles of  $\text{NiO}_x$  are partially covered with  $\text{MnO}_y$ . In image (E) ( $\text{NiO}_x/\text{MnO}_y/\text{GC}$  sample,  $\text{MnO}_y$  deposited first),  $\text{NiO}_x$  is extensively deposited compared with image (C). It seems also that  $\text{NiO}_x$  partially covers the previously deposited  $\text{MnO}_y$ . This means that the previously deposited  $\text{MnO}_y$  improves the interface properties in a way that enhances the deposition of  $\text{NiO}_x$ . Finally, it is clear that the order of deposition significantly affects the morphology of the deposited oxides.

It is well known from literatures that nickel oxide and not metallic nickel is the appropriate electrocatalyst for alcohol oxidation in alkaline medium [154, 155]. Hence the deposited nickel was passivated by the process described in Sec. 2.1.1 in order to convert Ni to  $\text{NiO}_x$ .

Fig. 2 compares cyclic voltammograms (CVs) of the (a) bare and the (b-e) modified GCE in 0.5 M NaOH solutions. The CV of the bare GCE (curve a) is featureless, as expected. At the  $\text{MnO}_y/\text{GC}$  electrode (curve b), a significant increase in the charging current is shown as a characteristic feature of  $\text{MnO}_y$ -modified electrodes; this featureless CV corresponds to the continuous change in the valences of Mn following the anodic and cathodic potential scanning [157]. At the  $\text{NiO}_x/\text{GC}$  electrode (curve c), the well-defined redox waves of the surface-confined Ni(II)/Ni(III) transformation is observed [158]. It has been reported that there are four possible phases produced over the anodic and cathodic scans for the nickel hydroxide electrode substrate, namely,  $\beta\text{-Ni}(\text{OH})_2$ ,  $\alpha\text{-Ni}(\text{OH})_2$ ,  $\beta\text{-NiOOH}$  and  $\gamma\text{-NiOOH}$  [153]. The transformations among the four phases can be identified well using the Bode diagram [159, 160]. The formation of  $\gamma\text{-NiOOH}$  phase is associated with the swelling or volume expansion of nickel film electrodes



**Fig. 1.** FE-SEM images of GCE (A), MnO<sub>x</sub>/GC (B), NiO<sub>x</sub>/GC (C), MnO<sub>x</sub>/NiO<sub>x</sub>/GC (D), and NiO<sub>x</sub>/MnO<sub>x</sub>/GC (E) electrodes.

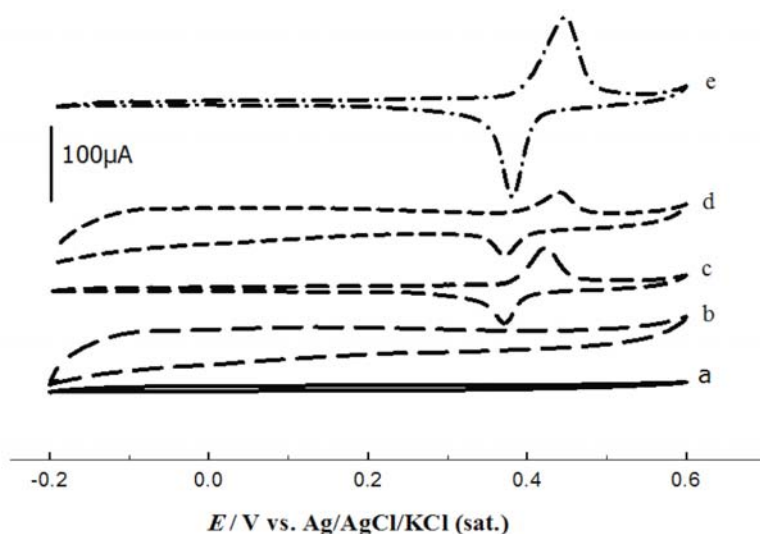
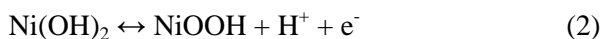


**Fig. 2.** CVs for different electrodes in 0.5 M NaOH solution; bare GC (a),  $\text{MnO}_y/\text{GC}$  (b)  $\text{NiO}_x/\text{GC}$  (c),  $\text{MnO}_y/\text{NiO}_x/\text{GC}$  (d) and  $\text{NiO}_x/\text{MnO}_y/\text{GC}$  (e). Scan rate = 100 mV/s.

with subsequent microcracks and disintegration. Lower inter-electrode spacing results in lower internal resistance and therefore better efficiency of the electrode for electrooxidation processes in alkaline medium [161, 162]. Therefore, the  $\beta$ -NiOOH phase is expected to be a better electroactive material for high electrochemical performance in alkaline solutions [161]. The Ni(II)/Ni(III) conversions occur via two pathways, by a proton diffusion mechanism in which  $\beta$ -NiOOH is likely formed (Eq. 2), and by a solvent mechanism in which  $\gamma$ -NiOOH is formed through the diffusion of  $\text{OH}^-$  (Eq. 3) [153].



Interestingly, in the case of the  $\text{MnO}_y/\text{NiO}_x/\text{GC}$  electrode (curve d), where  $\text{NiO}_x$  is deposited first, the current of the Ni(II)/Ni(III) couple significantly decreases in comparison with  $\text{NiO}_x/\text{GC}$  electrode; this is probably due to the partial deposition of  $\text{MnO}_y$  on the previously deposited  $\text{NiO}_x$  which is consistent with the SEM images shown in Fig. 1D.

For the  $\text{NiO}_x/\text{MnO}_y/\text{GC}$  electrode (curve e), where  $\text{MnO}_y$  is deposited first, we may conclude the following; the current of the Ni(II)/Ni(III) redox couple is markedly enhanced, the peak current is almost doubled as compared with  $\text{NiO}_x/\text{GC}$  (curve c).

The amount of the deposited Ni (estimated from I-t deposition curves), in the case of the  $\text{NiO}_x/\text{GC}$  and  $\text{NiO}_x/\text{MnO}_y/\text{GC}$  equal to 14.4 and 16.7  $\mu\text{g}$ , respectively. It is likely that the enhancement in the current of the Ni(II)/Ni(III) couple may be attributed to the increase of the  $\text{Ni}^{3+}$  content by doping the  $\text{NiO}_x$  with  $\text{MnO}_y$ . According to Das *et al.* [163], Mn(IV) can be converted during the anodic scan to a powerful and unstable oxidant, Mn(V), which can convert some of the  $\text{Ni}^{2+}$  to  $\text{Ni}^{3+}$  resulting in an increase in the conductivity of the former according to the following reaction.



### 2.1.3. Electrocatalytic oxidation of glucose at the modified electrodes

The glucose oxidation reaction at the GC and  $\text{MnO}_y/\text{GC}$  electrodes has been studied in our laboratory (data are not published). It was found that bare GCE is ineffective for the oxidation of glucose. While at the  $\text{MnO}_y/\text{GC}$  electrode, at the same conditions, the CV is characterized by large charging currents which is a characteristic feature of  $\text{MnO}_y$ -modified electrodes [155, 158]. However, on addition of glucose, the oxidation current is enhanced. It has been reported that glucose oxidation is electrocatalyzed at  $\text{MnO}_y$ -modified electrodes [161]. That is to say Mn(IV) is oxidized to Mn(V), then, in a subsequent chemical step, glucose is

oxidized according to Eq. 5, i.e., electrocatalytic (EC) mechanism.

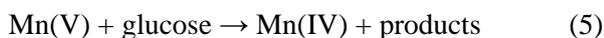
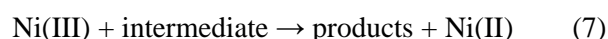


Fig. 3 shows linear scan voltammetry (LSV) responses obtained at the  $\text{NiO}_x/\text{GC}$ ; (a),  $\text{MnO}_y/\text{NiO}_x/\text{GC}$  (b) and  $\text{NiO}_x/\text{MnO}_y/\text{GC}$  (c) electrodes in 0.5 M NaOH solutions containing 20 mM glucose (inset shows the blank responses). At the  $\text{NiO}_x/\text{GC}$  electrode (curve a) glucose oxidation is markedly enhanced; glucose molecules adsorbed on the surface are oxidized at higher potentials coinciding with the oxidation of Ni(II) oxide. The oxidation of Ni(II) has the consequence of decreasing the number of sites for glucose adsorption, along with the poisoning effect of the products or intermediates formed during the reaction. This tends to decrease the overall rate of glucose oxidation. Thus, the anodic current passes through a maximum as the potential is anodically swept.

A number of mechanisms have been reported for the electrooxidation of alcohols on Ni in alkaline solutions. Those mechanisms can be summed up

into two ways; while Fleischmann *et al.* [150, 164] assumed catalytic/intermediate role for  $\text{NiOOH}$ , others [165-167] reported that methanol oxidation takes place after the complete conversion of  $\text{Ni(OH)}_2$  to  $\text{NiOOH}$  in the course of an anodic potential sweep. Hence we assume that a part of the anodic current is due to glucose oxidation by  $\text{NiOOH}$  and the other part of the current is due to glucose oxidation on the surface of the oxide layer by direct electrooxidation.

The first step in the whole process is the redox transition of nickel species from Ni(II) to Ni(III), followed by the second step which is the glucose oxidation on the modified surface via the following reactions:



The Ni(III) sites are regenerated by the anodic potential afforded by the power source. Glucose oxidation can also take place on the  $\text{NiOOH}$  surface by direct electrooxidation [166, 167]:

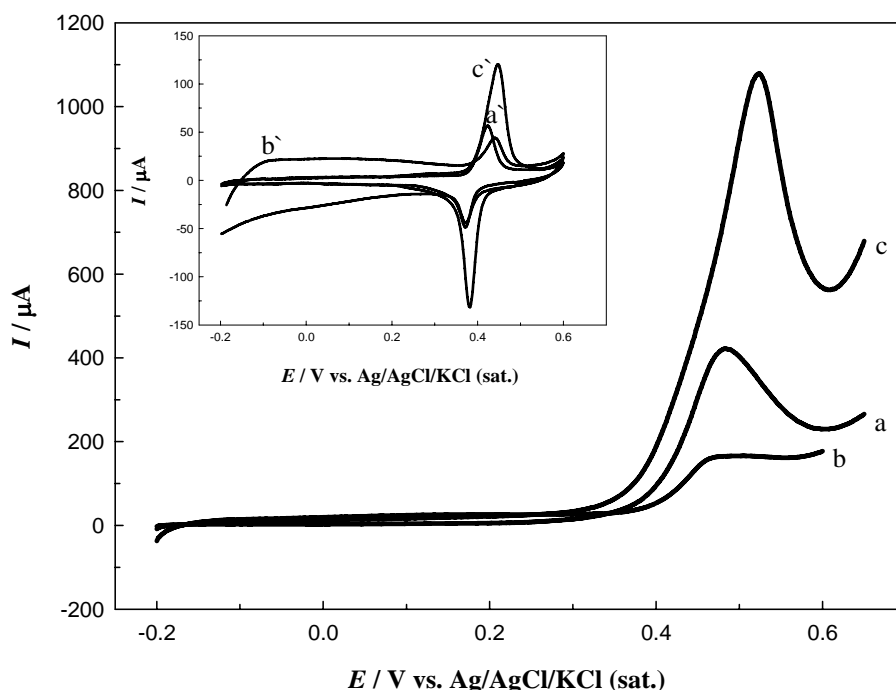
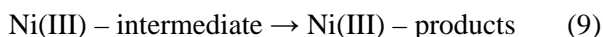


**Fig. 3.** LSV responses obtained at (a)  $\text{NiO}_x/\text{GC}$ , (b)  $\text{MnO}_y/\text{NiO}_x/\text{GC}$  and (c)  $\text{NiO}_x/\text{MnO}_y/\text{GC}$  electrodes in 0.5 M NaOH solutions containing 20 mM glucose at a scan rate 100 mV/s. Inset shows CV responses obtained at (a')  $\text{NiO}_x/\text{GC}$ , (b')  $\text{MnO}_y/\text{NiO}_x/\text{GC}$  and (c')  $\text{NiO}_x/\text{MnO}_y/\text{GC}$  electrodes in glucose-free 0.5 M NaOH solution at a scan rate of 100 mV/s.



Equations (6) and (7) are according to the Fleischmann mechanism [149, 165], and in Eqs. (8) and (9),  $\text{Ni}^{3+}$  is used as an active surface for glucose oxidation. Gluconolactone [167, 168] as well as methanoates and oxalates [169, 170] have been reported as the oxidation products of glucose electrooxidation.

Recalling Fig. 3 in which the glucose oxidation at  $\text{MnO}_y/\text{NiO}_x/\text{GC}$  and  $\text{NiO}_x/\text{MnO}_y/\text{GC}$  electrodes in 0.5 M NaOH is shown as curves b and c, respectively, it is obvious that the order of the deposition of the nano- $\text{MnO}_y$  and  $\text{NiO}_x$  dramatically affects the performance of the binary catalyst. For instance, the peak current for glucose oxidation is much higher in the case of  $\text{NiO}_x/\text{MnO}_y/\text{GC}$  and the onset potential of glucose oxidation shifted to less positive values in the case of  $\text{NiO}_y/\text{MnO}_y/\text{GC}$  (c) compared to  $\text{MnO}_y/\text{NiO}_x/\text{GC}$  (b). When the  $\text{MnO}_y/\text{NiO}_x/\text{GC}$  is used ( $\text{NiO}_x$  is deposited first) (curve b) the electroactivity significantly decreases. However, the highest response is obtained on the  $\text{NiO}_x/\text{MnO}_y/\text{GC}$  electrode, i.e., when  $\text{MnO}_y$  is deposited first, followed by the electrodeposition of  $\text{NiO}_x$ . The larger response at the binary catalyst  $\text{NiO}_x/\text{MnO}_y/\text{GC}$  in comparison with  $\text{NiO}_x/\text{GC}$  electrode may be the result of two factors; first, glucose is expected to be adsorbed quite easily on  $\text{MnO}_y$  due to the possibility of hydrogen bond formation using the multiple hydroxyl groups present in the molecule [169, 171]. Thus the accessibility of glucose at the electrode surface increases. Second,  $\text{MnO}_y$  plays a significant role;  $\text{Ni}^{2+}$  can be oxidized to  $\text{Ni}^{3+}$  by the strong oxidant  $\text{Mn(V)}$ , which increases the concentration of  $\text{Ni}^{3+}$  in the matrix. As a result of this, the conductivity of the matrix increases and this leads to enhancement of the glucose oxidation [170, 171].

#### 2.1.4. Effect of the loading level of $\text{NiO}_x$

Fig. 4 compares linear scan voltammograms of  $\text{NiO}_x/\text{GC}$  (A), and  $\text{NiO}_x/\text{MnO}_y/\text{GC}$  (B) electrodes, at different loading levels of deposited  $\text{NiO}_x$  in 0.5 M NaOH solution containing 20 mM glucose.  $\text{MnO}_y$  loading is kept constant at 60 cycles for all experiments.  $\text{NiO}_x$  and  $\text{MnO}_y$  were electrodeposited as described in Sec. 2.1.1. As mentioned above,

$\text{NiO}_x$  is responsible for the electrocatalytic oxidation of glucose due to the presence of the  $\text{Ni(II)/Ni(III)}$  redox couple; smaller loadings of the  $\text{NiO}_x$  at the GCE results in a significant enhancement in the electrocatalytic activity of the GCE for glucose oxidation. At both electrodes, as the loading level of  $\text{NiO}_x$  increases, the peak current of glucose oxidation increases and the onset potential shifts to lower positive values.

The effect of scan rate on the electrooxidation of glucose at the optimum loading level was studied in our laboratory (data not published), and it was found that, at scan rates larger than  $100 \text{ mVs}^{-1}$ , the  $I_p/v^{1/2}$  function does not change significantly with the scan rate. The above observation is a characteristic feature of catalytic reactions [171, 172]. It becomes clear that the deposition of  $\text{NiO}_x$  onto the  $\text{MnO}_y/\text{GC}$ -modified electrode significantly enhances the glucose electrooxidation due to two considerations; first,  $\text{MnO}_y$  enhances the adsorption of glucose and the second is the mediation by the second oxide ( $\text{NiO}_x$ ) in an EC mechanism as represented by Eqs. 5 and 6 and confirmed by the  $I_p/v^{1/2} - v$  relation.

In order to get further insight, Tafel plot of  $E$  vs.  $\log I$  was plotted using the rising part of the current-voltage data, i.e., in the potential range 0.35-0.45 V (Fig. 3), at a scan rate of  $5 \text{ mVs}^{-1}$  for a 0.5 M NaOH containing 20 mM glucose (Fig. 5). Tafel slopes for  $\text{NiO}_x/\text{GC}$  (a),  $\text{MnO}_y/\text{NiO}_x/\text{GC}$  (b), and  $\text{NiO}_x/\text{MnO}_y/\text{GC}$  (c) were found to be equal to 108.44, 115.25 and 113.54  $\text{mV decade}^{-1}$ , respectively. The similarity of the Tafel slopes (average value ca.  $112 \text{ mV decade}^{-1}$ ) for the different electrodes indicates that the glucose oxidation proceeds via a common rate-determining step in all the cases, which is the one-electron transfer step (Eq. 6).

#### 2.1.5. Long-term stability of the prepared electrocatalysts

One of the main objectives of using the binary oxide of  $\text{NiO}_x$  and  $\text{MnO}_y$  is to enhance the stability of the  $\text{NiO}_x$  (the active oxide)-modified GCE. Hence, to investigate the stability of the proposed catalysts, current-time curves were recorded for glucose oxidation at the proposed electrodes at a constant potential of 0.5 V and 0.52 V for  $\text{NiO}_x/\text{GC}$  (a), and  $\text{NiO}_x/\text{MnO}_y/\text{GC}$  (b)

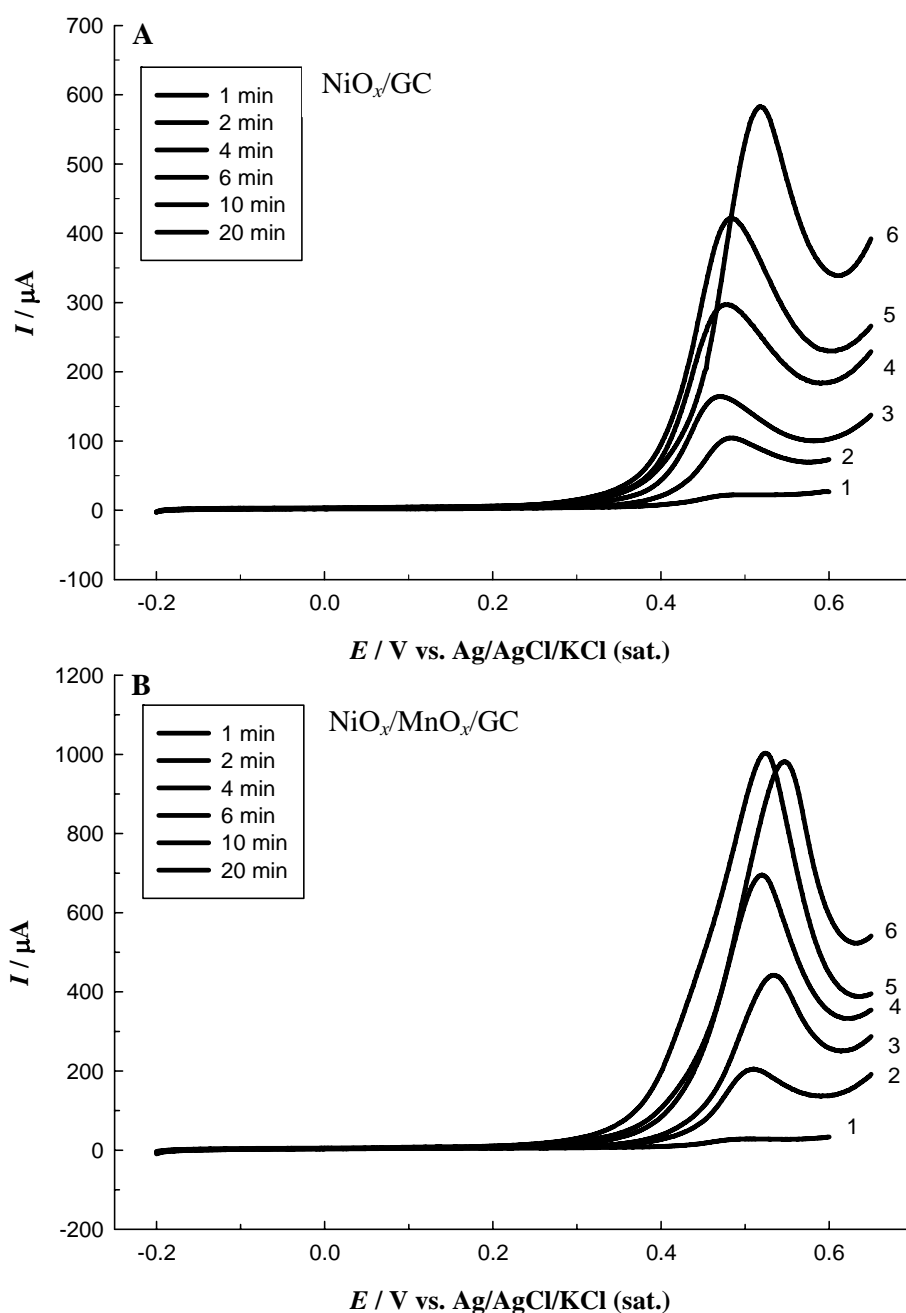


**Fig. 4.** LSV response obtained at (A) NiO<sub>x</sub>/GC and (B) NiO<sub>x</sub>/MnO<sub>y</sub>/GC electrodes with different loading levels of NiO<sub>x</sub> in 0.5 M NaOH solutions containing 20 mM glucose at a scan rate of 100 mV/s. In panel (B) the MnO<sub>y</sub> loading is fixed at 60 cycles of MnO<sub>y</sub> deposition.

electrodes, respectively and the data are shown in Fig. 6. The figure depicts that the NiO<sub>x</sub>/MnO<sub>y</sub>/GC electrode supports higher oxidation currents than that obtained at the NiO<sub>x</sub>/GC electrode. This level of enhancement could still be observed after three hours of continuous measurement. This indicates

a better mechanical stability and good adhesion among the coexisting oxides.

#### 2.1.6. Tolerance of glucose electrocatalytic oxidation

Generally, using non-enzymatic sensors for the analysis of glucose often suffers from drawbacks

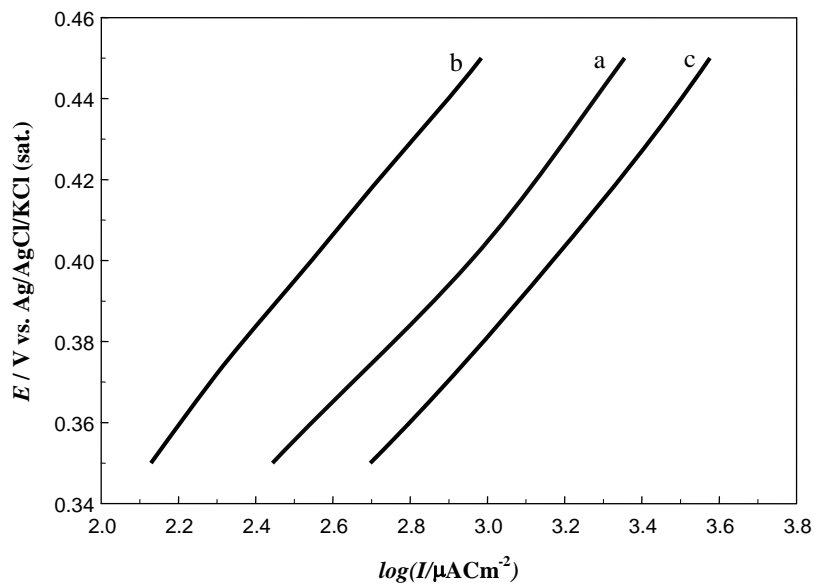


**Fig. 5.** Tafel plots for (a) NiO<sub>x</sub>/GC, (b) MnO<sub>y</sub>/NiO<sub>x</sub>/GC and (c) NiO<sub>x</sub>/MnO<sub>y</sub>/GC electrodes in 0.5 M NaOH solution containing 20 mM glucose at a scan rate 5 mV/s.

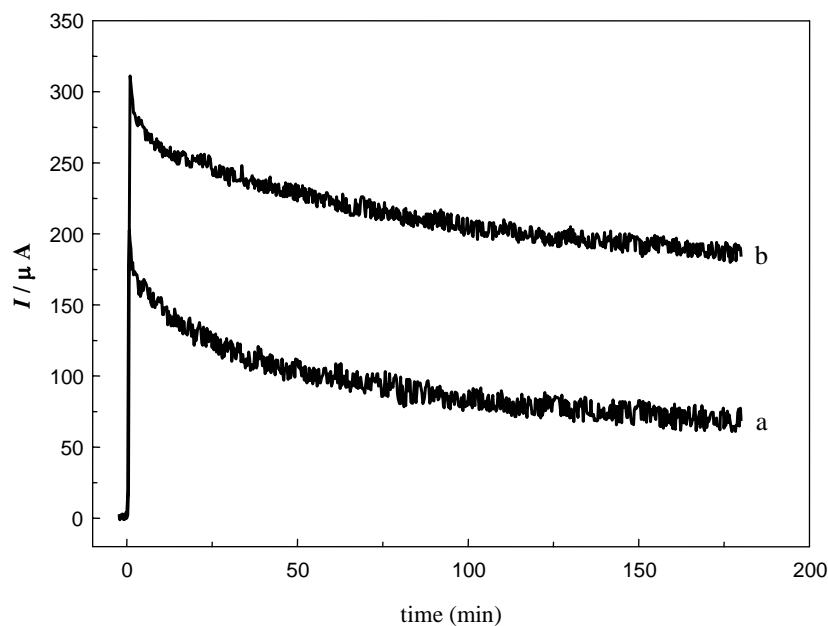


**Fig. 6.** Current-time relation obtained during glucose oxidation at (a) NiO<sub>x</sub>/GC and (b) NiO<sub>x</sub>/MnO<sub>y</sub>/GC electrodes in 0.5 M NaOH containing 20 mM glucose at (a) 0.5 V and (b) 0.52 V, respectively.

of low sensitivity and interference of other oxidizable components such as ascorbic acid and uric acid [173]. The adsorption of chlorides, which decreases significantly the operational stability is another challenge. It has been reported that CuO<sub>x</sub>-modified electrodes are good non-enzymatic catalysts for

glucose oxidation in alkaline medium, and thus the poisoning by chloride at this modified electrode has been extensively studied [173]. High tolerance of NiO<sub>x</sub>/MnO<sub>y</sub>/GC binary catalysts towards poisoning products resulting from glucose oxidation and also towards poisoning by halide ions has been

reported by our group [153]. In this report it has been shown that the  $\text{NiO}_x/\text{MnO}_y/\text{GC}$  electrode presents a superior electrocatalytic activity compared with  $\text{NiO}_x/\text{GC}$  electrode, and a comparable behavior to  $\text{NiO}_x/\text{GC}$  electrode regarding the tolerance to poisoning by halides, even in the presence of high concentrations of  $\text{Cl}^-$  and  $\text{Br}^-$  up to 0.3 M. On the other hand it was found that iodide ions had a significant effect on glucose electrooxidation even at lower concentrations than the other two halide ions.

### 2.1.7. Poisoning effect of chloride and bromide ions

In our work [154], responses of  $\text{NiO}_x/\text{MnO}_y/\text{GC}$  electrode were recorded for glucose electrooxidation in the presence of different concentrations of chloride and bromide ions, ranging from 0.1 M to 0.3 M. Interestingly, it has been found that the effect of adding chloride or bromide ions, even at higher concentrations, is negligible [154]. This indicates that the proposed binary catalyst exhibits good resistance to surface fouling and is a promising electrocatalyst for the development of enzymeless glucose sensors and alkaline fuel cells at low cost. It has been reported [173] that  $\text{NiO}_x/\text{GC}$  electrode has a strong tolerance to chloride ions, consistent with our results [154]. However, the  $\text{NiO}_x/\text{MnO}_y/\text{GC}$  electrode has the advantage of higher electrocatalytic activity compared to the  $\text{NiO}_x$  electrode [173].

Consecutive LSV responses for the forward and backward scans were obtained at  $\text{NiO}_x/\text{MnO}_y/\text{GC}$  electrode in 0.5 M NaOH containing 20 mM glucose with either 0.1 M  $\text{Cl}^-$  or 0.1 M  $\text{Br}^-$  [154]. To quantitatively compare the poisoning effect of  $\text{Cl}^-$  and  $\text{Br}^-$  ions, the oxidation peak currents for the forward scan in the halide-free glucose and after adding  $\text{Cl}^-$  and  $\text{Br}^-$  are plotted as a function of the number of potential cycles as shown in Fig. 7. The following inferences can be obtained from Fig. 7:

- (i) In the presence of  $\text{Cl}^-$  or  $\text{Br}^-$  ions, the oxidation peak currents for the first cycle are similar to that in the absence of both species. During potential cycling the peak current decreases in the presence of any of the above halide ions, albeit to different extent.
- (ii) The decreasing rate of the oxidation peak current follows the sequence:  $\text{Br}^- > \text{Cl}^- > \text{halide-free}$  (glucose only). This behavior is due to the differences in the electronegativity of  $\text{Cl}^-$  and  $\text{Br}^-$  ions, ionic radii and solvation ability [174].
- (iii) The peak current changes with the number of potential scan cycles. However, the recovery of the electrode activity in the presence of  $\text{Cl}^-$  is faster than in the presence of  $\text{Br}^-$ . Note that in the presence of  $\text{Cl}^-$ , the initial peak current is completely recovered, while in the case of  $\text{Br}^-$  it is not.

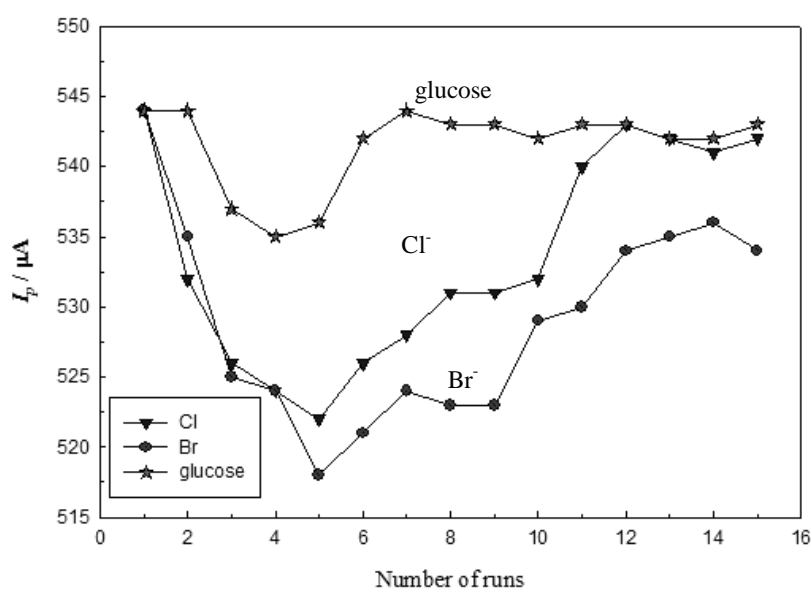


Fig. 7. The relationship between peak current at each run and number of runs.

- (iv) The largest decrease in the peak current is about 22  $\mu\text{A}$  for the  $\text{Cl}^-$  ions and 26  $\mu\text{A}$  for the  $\text{Br}^-$  ions, i.e., 4.0% and 4.7% from the original current, respectively.

The above results reveal the tolerance of  $\text{NiO}_x/\text{MnO}_y/\text{GC}$  electrode to poisoning by chloride and bromide ions at  $\text{NiO}_x/\text{MnO}_y/\text{GC}$  electrodes during glucose oxidation. This may be attributed to the low adsorbability and high solvation of the  $\text{Cl}^-$  and  $\text{Br}^-$  ions. It could also be attributed to the high reversible oxidation potentials of  $\text{Cl}_2/\text{Cl}^-$  and  $\text{Br}_2/\text{Br}^-$  reactions (1.36 and 1.06 V, respectively vs. standard hydrogen electrode (SHE) [175].

#### 2.1.8. Effect of iodide ion

Fig. 8 shows the consecutive LSV responses for the forward scans (I) and backward scans (II) obtained at the  $\text{NiO}_x/\text{MnO}_y/\text{GC}$  electrode in 0.5 M NaOH containing 20 mM glucose and different iodide ion concentrations ranging from  $10^{-5}$  to  $10^{-2}$  M. Note that, the concentration range used for the effect of iodide is much lower than that used above for  $\text{Cl}^-$  and  $\text{Br}^-$ . This is because  $\text{I}^-$  has significant adsorbability and so, at high concentrations it blocks the electrode surface active sites.

In the case of the iodide-free glucose solution (curve a), the forward scan current corresponds to the combination of two reactions, that is, oxidation of  $\text{Ni}^{2+}$  to  $\text{Ni}^{3+}$  and glucose electrooxidation by interaction with  $\text{Ni}^{3+}$ . The backward scan corresponds to the combination of  $\text{Ni}^{3+}$  reduction to  $\text{Ni}^{2+}$  and the glucose electrooxidation with the already present  $\text{Ni}^{3+}$  [154, 155, 176].

It has been reported that iodide ion is oxidatively adsorbed at Pt and Au electrodes as a zero-valent atomic iodine at potentials between -0.4 V and +0.4 V (Ag/AgCl reference) [177]. The amount of the adsorbed iodine increases upon scanning the potential to more positive values than -0.4 V until the surface is saturated with a monolayer of close-packed iodine atoms of coverage limited by Van der Waals interactions. Additional iodine atoms forced into the already space-limited interfacial layer leads to the formation of molecular iodine, which evolves into the solution as aqueous  $\text{I}_2$  ( $2 \text{I}^- \leftrightarrow \text{I}_2 + 2\text{e}^-$ ). At the surface of Pt and Au anode, at considerably higher positive potentials and before oxygen evolution, the zero-valent adsorbed iodine is oxidized to aqueous iodate

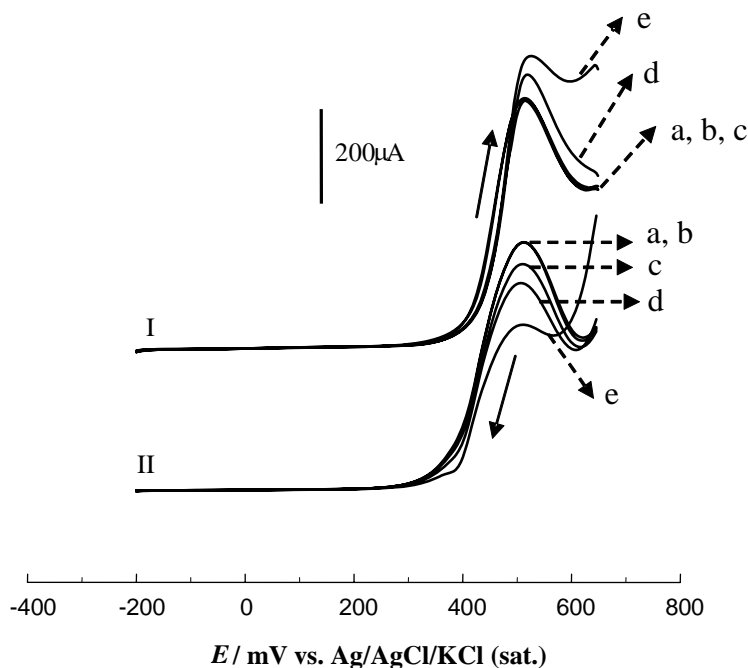


**Fig. 8.** Consecutive LSV responses for the forward scan (I) and backward scan (II) obtained at  $\text{NiO}_x/\text{MnO}_y/\text{GC}$  electrode in 0.5 M NaOH containing 20 mM glucose at different iodide ion concentrations. (a) 0.0, (b)  $10^{-5}$ , (c)  $10^{-4}$ , (d)  $10^{-3}$  and (e)  $10^{-2}$  M. Scan rate:  $100 \text{ mVs}^{-1}$ .

( $I_2 \leftrightarrow IO_3^-$ ) along with the oxide formation on the electrode surface. Finally, it is quite probable that the iodates formed at the electrode diffuses back into the solution and react with the iodide, forming iodine again [178, 179].

In Fig. 8, upon the addition of the iodide ions, a significant effect appears in the forward and backward scans at each concentration (curves b-d). In the presence of  $10^{-5}$  M  $I^-$  (curve b), the LSV for the forward and backward scans are similar to that of iodide-free glucose solution (curve a), and there is no significant change in both the forward and backward scan. In curve c ( $10^{-4}$  M  $I^-$ ), again the forward scan is similar to the case of iodide-free glucose solution, while the backward current is lower than the iodide-free glucose solution (curve a). The forward scan current does not decrease as is expected from the poisoning effect by iodide. This can be explained as follows: the anodic current is a combination of two processes; the oxidation of glucose and the oxidation of the adsorbed  $I_2$  to  $IO_3^-$ . The decrease in the current corresponding to glucose oxidation due to poisoning is compensated by the oxidation of the adsorbed  $I_2$  to  $IO_3^-$ . Hence the current in the forward scan is kept almost unchanged. On the other hand, the

decrease in the backward current in the presence of iodide ions might be attributed to the adsorption of iodine or iodates formed in the forward scan that blocks some of the active sites. Another factor is the presence of another reduction reaction for iodide derivatives in parallel with the  $Ni^{3+}$  reduction, and the combination of these two processes can decrease the overall back-oxidation current of glucose in the backward scan, and hence glucose oxidation current in the backward scan decreases in comparison with the case of iodide-free glucose solution.

In the case of  $10^{-3}$  M  $I^-$  (curve d), the forward scan current is higher than the iodide-free glucose solution case and the backward scan current is lower than iodide-free glucose case (curve a). The increase of current in the forward scan may be attributed to the oxidation of the adsorbed zero-valent iodine to aqueous iodine atoms and/or iodates as they are available in the present potential range as revealed in Fig. 9 (curve d), in which the CV responses obtained at the  $NiO_x/MnO_y/GC$  in 0.5 M NaOH at different  $I^-$  concentrations is shown. The current increases in the potential range between 0.4 to 0.6 V at  $NiO_x/MnO_y/GC$  during the forward scan in the presence of  $10^{-3}$  M  $I^-$ . The decrease in the backward scan current (Fig. 8, curve d) is attributed to the same reasons as in the case of

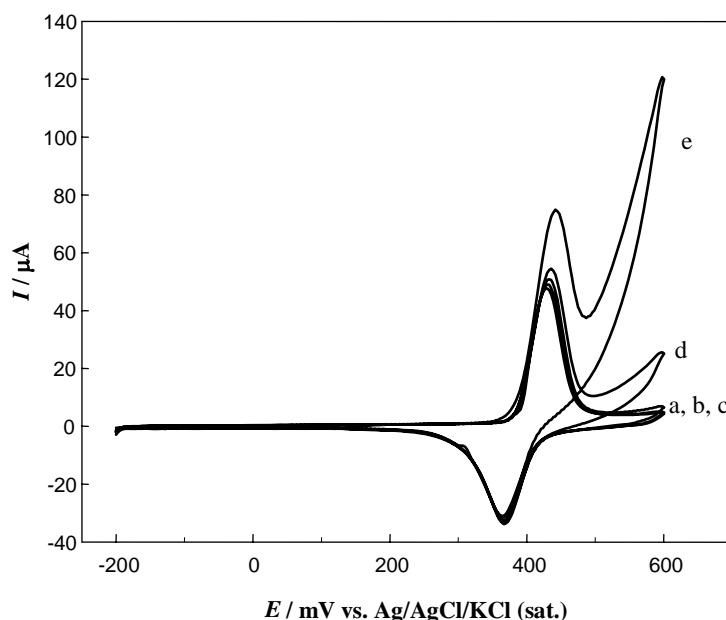


**Fig. 9.** CV responses obtained at  $NiO_x/MnO_y/GC$  electrode in 0.5 M NaOH at different  $I^-$  concentrations. (a) 0.0, (b)  $10^{-5}$ , (c)  $10^{-4}$ , (d)  $10^{-3}$  and (e)  $10^{-2}$  M. Scan rate:  $100 \text{ mVs}^{-1}$ .

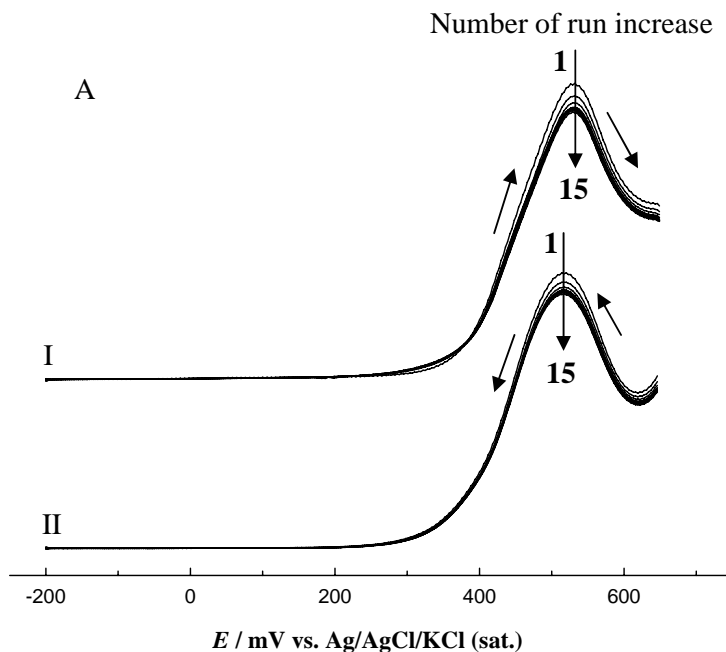
$10^{-4}$  M I $^-$ . However the decrease in the backward scan current in the present case is more significant as the adsorbed species in the forward scan is higher in the present case compared with the case of  $10^{-4}$  M I $^-$ .

In the case of  $10^{-2}$  M I $^-$  (curve e), where the concentration of iodide ions becomes close to glucose concentration, the transformation from adsorbed iodine to aqueous iodine and/or iodates become more considerable. Thus, the current of the forward scan becomes higher than that of the iodide-free glucose solution case and lower than the case of  $10^{-3}$  M I $^-$ . The increase in the current in curve e in Fig. 9 covers a wide potential range from the onset potential of the peak to 0.65 V, in accordance with that found in Fig. 8 where no glucose was added. The increase in the current in the forward scan in the presence of  $10^{-2}$  M I $^-$  is not much higher than in the case of  $10^{-3}$  M I $^-$ , which could be attributed to the fact that glucose oxidation is more inhibited in the forward scan than in the case of  $10^{-3}$  M I $^-$ , and hence the current difference between the case of  $10^{-3}$  M and  $10^{-2}$  M I $^-$  in the presence of glucose is negligible. In the backward scan (Fig. 8 (curve e)), the peak current becomes much lower than in the case of  $10^{-3}$  M I $^-$ ,

as the poisoning in this case is much higher than cases of  $10^{-3}$  and  $10^{-4}$  M I $^-$ .

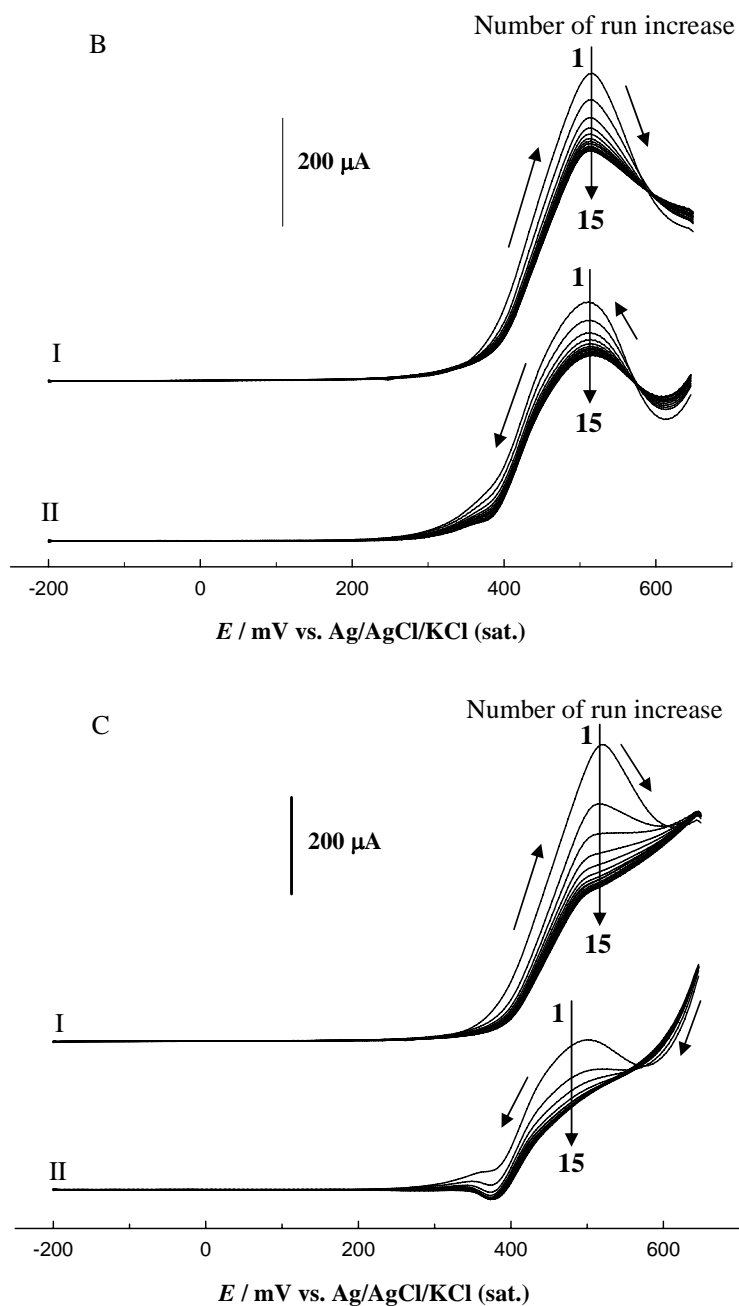
Figs. 10(A), 10(B) and 10(C) show consecutive LSV responses for the forward scan (I) and backward scan (II) obtained at NiO $_x$ /MnO $_y$ /GC electrode in 0.5 M NaOH containing 20 mM glucose and  $10^{-4}$  (A),  $10^{-3}$  (B), and  $10^{-2}$  (C) M I $^-$ , respectively. We can see that with increase in the number of potential scan cycles, both the forward and backward currents decrease, and this decrease depends on the iodide concentration. In addition, in cases (B) and (C), with the increase in the concentration of the I $^-$ , a small peak appears in the backward scan (II) with the increase in the number of potential scan cycles especially in the latter case. That peak may be attributed to the reduction of the remaining NiOOH, as the surface poisoning by iodates and iodine hinder glucose from interacting with Ni $^{3+}$ .

Fig. 11 shows the relationship between the peak current for the forward scan ( $I_p$ ) with the number of potential scan cycles (data were taken from Fig. 10). This figure demonstrates an interesting drop in the oxidation peak current with increase in the potential sweep number and with increase in the I $^-$  concentration. It is worth mentioning that



**Fig. 10**

Fig. 10 continued..



**Fig. 10.** LSV responses for the forward scan (I) and backward scan (II) obtained at NiO<sub>x</sub>/MnO<sub>y</sub>/GC electrode in 0.5 M NaOH containing 20 mM glucose at different I<sup>-</sup> concentrations: 10<sup>-4</sup> (A), 10<sup>-3</sup> (B) and 10<sup>-2</sup> (C) M at a scan rate 100 mVs<sup>-1</sup>.

the peak current for the first run in cases (c) and (d) (Fig. 11) is higher than the blank (0.5 NaOH) itself (curve a). This behavior was attributed to the adsorbed iodine as it is available in the present

potential range. In the subsequent potential scan cycles, the peak current decreases with the increase in the potential scan number to values lower than that of the blank. The fact that the peak

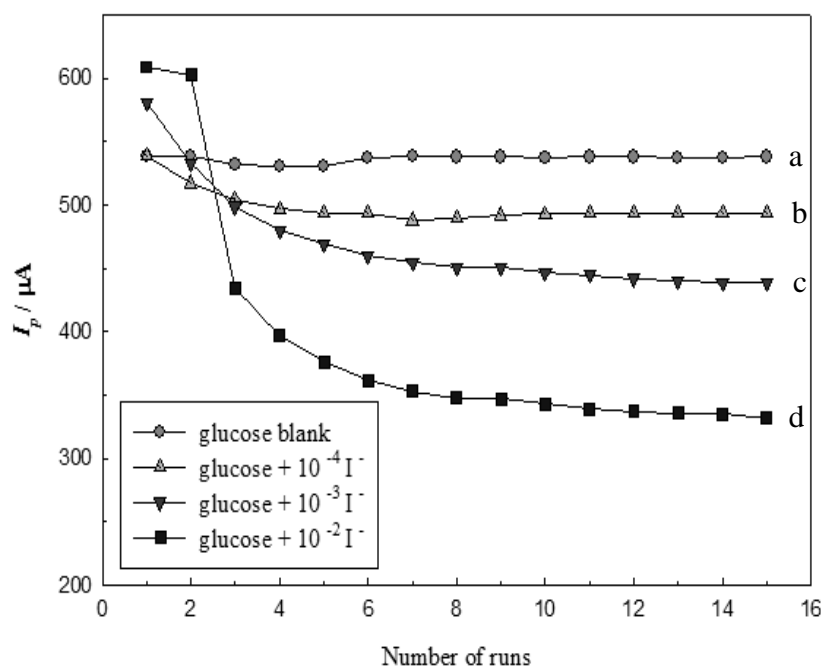


**Fig. 11.** The relationship between peak current for the forward scan at each run and number of runs (data were taken from Fig.10).

current decreases again after the first run although two reactions occur (glucose oxidation and adsorbed iodine oxidation), could be explained by considering the cross effect of both glucose and  $\text{I}^-$  oxidation on each other. That is to say, the glucose oxidation reaction is retarded by the adsorbed products of iodine oxidation and the glucose oxidation reaction may retard further oxidation of  $\text{I}^-$  to  $\text{I}_2$ . In Fig. 11 the three curves in the presence of  $\text{I}^-$  ions exhibit a two-decay stage, an initial rapid stage which depends on the concentration of  $\text{I}^-$  ion followed by a slow one. During the initial decay, the glucose oxidation peak current ( $I_p$ ) rapidly falls to ca. 90.0, 84.4, and 65.4% of its original value, for (b), (c) and (d), respectively, suggesting a quick poisoning process especially with the high  $\text{I}^-$  concentration. In the slow stage the decrease in the peak current is negligible. For instance for case (d), the peak current decreases from 343  $\mu\text{A}$  to 332  $\mu\text{A}$ , i.e., about 11  $\mu\text{A}$  decrease, which is about 2% decrease from the initial current value.

It becomes clear that the poisoning effect of chloride and bromide ions differs greatly from the poisoning effect of iodide ion, and this difference may be attributed to the difference in their adsorbability and reactivity. It is likely that the

radii and the electronegativity of the halide ions have a profound influence on their adsorption process. Electronegativity increases from  $\text{I}^-$  to  $\text{Cl}^-$  ( $\text{I}^- = 2.5$ ,  $\text{Br}^- = 2.8$ ,  $\text{Cl}^- = 3.0$ ) while atomic radius decreases from  $\text{I}^-$  to  $\text{Cl}^-$  ( $\text{I}^- = 135$  pm,  $\text{Br}^- = 114$  pm,  $\text{Cl}^- = 90$  pm). Hence, the iodide ion is more predisposed to adsorption than the bromide and chloride ions, and this is a reason behind the difference in their poisoning effect [174]. In addition to these, from the thermodynamic point of view, potentials for the reversible  $\text{Cl}_2/\text{Cl}^-$ ,  $\text{Br}_2/\text{Br}^-$  and  $\text{I}_2/\text{I}^-$  reactions are, respectively, 1.36, 1.06 and 0.54 V vs. SHE. This also explains why chloride and bromide ions do not affect glucose oxidation reaction even at these high concentrations. While for the iodide ion, the state is very different as the iodide can be oxidized easily to iodine or iodates that are also possible in the present experimental conditions [175, 178, 179].

## 2.2. Single catalyst at electrochemically activated GC substrate

Many articles have been published in the area of using single catalysts such as  $\text{NiO}_x$ -modified GC electrode in the electrocatalytic oxidation of glucose [156, 180-184].  $\text{NiO}_x$  is usually deposited on

unmodified GC electrodes. In this part, we examine [156], the effect of anodic oxidation of glassy carbon (GC) electrode on the deposition of nickel oxide ( $\text{NiO}_x$ ) nanoparticles and the electrocatalytic oxidation of glucose on the thus prepared modified electrode. In our work [156], the GC was pretreated by anodic oxidation in 0.1 M  $\text{H}_2\text{SO}_4$  solution at different anodic potentials for different time periods. Different shapes and sizes of  $\text{NiO}_x$  nanoparticles were obtained when  $\text{NiO}_x$  was deposited on anodically-oxidized GC electrode. The purpose of the anodic oxidation was to manipulate the GC surface such that it gave higher surface concentration of C-O functional groups and higher surface area, which leads to an extraordinary increase in the activity of  $\text{NiO}_x$  for glucose electrooxidation [156].

Usually, preparation of  $\text{NiO}_x$  for electrochemical applications using different techniques is performed on ordinary untreated glassy carbon (GC) electrodes. Such techniques include sol-gel preparation of powder  $\text{NiO}_x$  followed by casting [180], electrodeposition [181] and other techniques [96, 182].

Functional groups have been shown to be responsible for the electrochemical activity of carbonaceous surfaces by providing electrochemically-active surface sites on them. For increasing the reactivity of carbon electrodes, "activation" has been used frequently to avoid adsorption of impurities; increase of surface area entails the formation of particular active sites on the carbon surface. Several activation methods have been used for the GC surface. These methods include electrochemical pretreatment (ECP) [183-186], laser irradiation [185-187], vacuum heat treatment (VHT) [188] and ultraclean polishing [189]. The mechanisms of GC activation procedures are related with surface cleaning, oxide film formation, formation of graphite edge planes, and changes in the microscopic surface involved [185, 190, 191]. Oxidation of GC is known to enhance its electrocatalytic properties in many applications such as electrochemical oxidation of many organic molecules [192-195]. For instance, Jovanović *et al.*, [193-195] published a series of articles on the oxidation of small organic molecules on an oxidized GC-modified electrode with Pt nanoparticles. They attributed the enhancement of the electrooxidation of such molecules to the increase in the surface area and creation of C-O functional groups on the GC substrate. While the

effects of GC pretreatment by anodic oxidation on the electrooxidation of some of the smaller organic molecules have been studied [193-195], none has studied such effects on the glucose electrocatalytic oxidation albeit of equal importance.

In this part, we discuss the effects of surface modification of glassy carbon substrate via its anodic pretreatment, on the electrodeposition of  $\text{NiO}_x$  nanoparticles and electrocatalytic properties of  $\text{GC}_{\text{ox}}/\text{NiO}_x$  for oxidation of glucose in alkaline solution. In our work [157], GC was oxidized in 0.1 M of  $\text{H}_2\text{SO}_4$  at 1.0, 1.5 and 2.0 V for different time periods (60, 120 and 300 s, respectively). The oxidized GC ( $\text{GC}_{\text{ox}}$ ) was modified with  $\text{NiO}_x$  as discussed above.

### 2.2.1. Morphological characterizations

$\text{GC}/\text{NiO}_x$  and  $\text{GC}_{\text{ox}}/\text{NiO}_x$  electrodes were characterized [157] by microscopic and electrochemical techniques i.e., by SEM, energy-dispersive X-ray spectroscopy (EDX) and cyclic voltammetry (CV). The SEM images (Fig. 12A, and B) demonstrate the morphology of glassy carbon surface before oxidation, (A) GC, and after oxidation, (B)  $\text{GC}_{\text{ox}}$ , of the GC in 0.1 M of  $\text{H}_2\text{SO}_4$  at 2 V for 300 s. Image (B) clearly shows rough surface of the  $\text{GC}_{\text{ox}}$  compared to image (A) (GC). This is evidence on the increase in the GC surface area due to surface oxidation.

EDX chart for GC before and after anodic oxidation (at 2 V for 300 s) were taken at the same conditions as cited in captions of Fig. 12A, and B. The percent of carbon and oxygen at the surface of glassy carbon electrode before and after activation of the surface is shown in Table 1. Formation and growth of oxide layer at the  $\text{GC}_{\text{ox}}$  surface compared with GC surface (without activation) is evident from Fig. 12 and Table 1. The increase in the percentage of oxygen (O%) in the case of  $\text{GC}_{\text{ox}}$  with respect to GC is due to the formation of C-O functional groups with the oxidation of the GC. The above increase in the C/O ratio is in accordance with an X-rays photon spectroscopy (XPS) spectrum measured for an anodically-oxidized GC under similar conditions [196].

Fig. 13 presents SEM images of  $\text{GC}/\text{NiO}_x$  (A) and  $\text{GC}_{\text{ox}}/\text{NiO}_x$  (B). The images show the morphology and particle size distribution of the  $\text{NiO}_x$  on the surface of GC before activation (A)

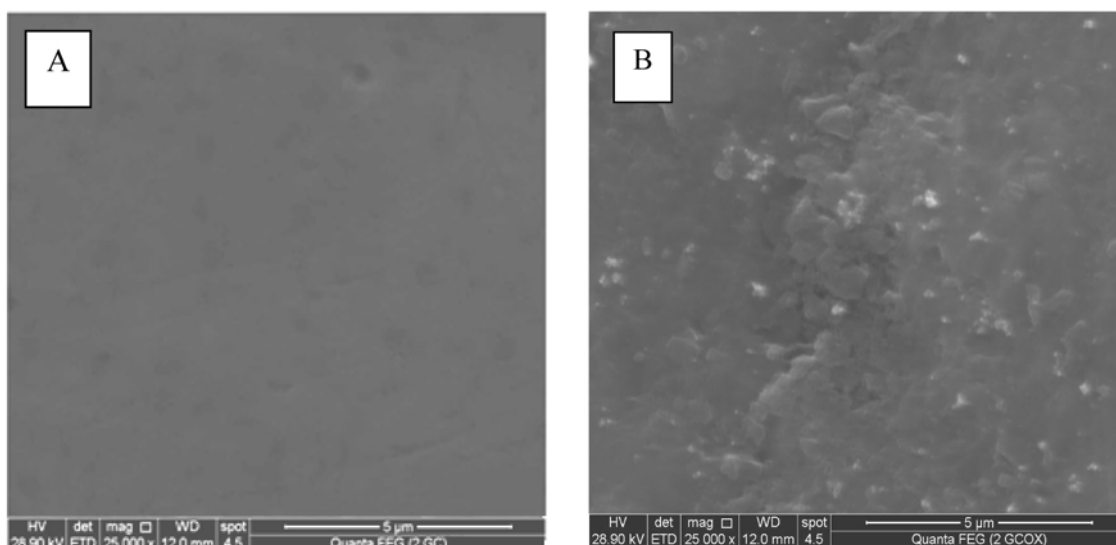


**Fig. 12.** FE-SEM images of GC (A) and GC<sub>ox</sub> (B). The GC<sub>ox</sub> was prepared by oxidation of GC at 2 V in 0.1 M H<sub>2</sub>SO<sub>4</sub> for 300 s.

**Table 1.** The percent of oxygen and carbon obtained from EDX charts of GC and GC<sub>ox</sub>. The GC<sub>ox</sub> was prepared by oxidation of GC at 2 V in 0.1 M H<sub>2</sub>SO<sub>4</sub> for 300 s. The peak of carbon and oxygen appears at the same energy peak for both GC and GC<sub>ox</sub> but with different percentages.

Type of electrode	GC	GC <sub>ox</sub>
%C	97	90
%O	3	10

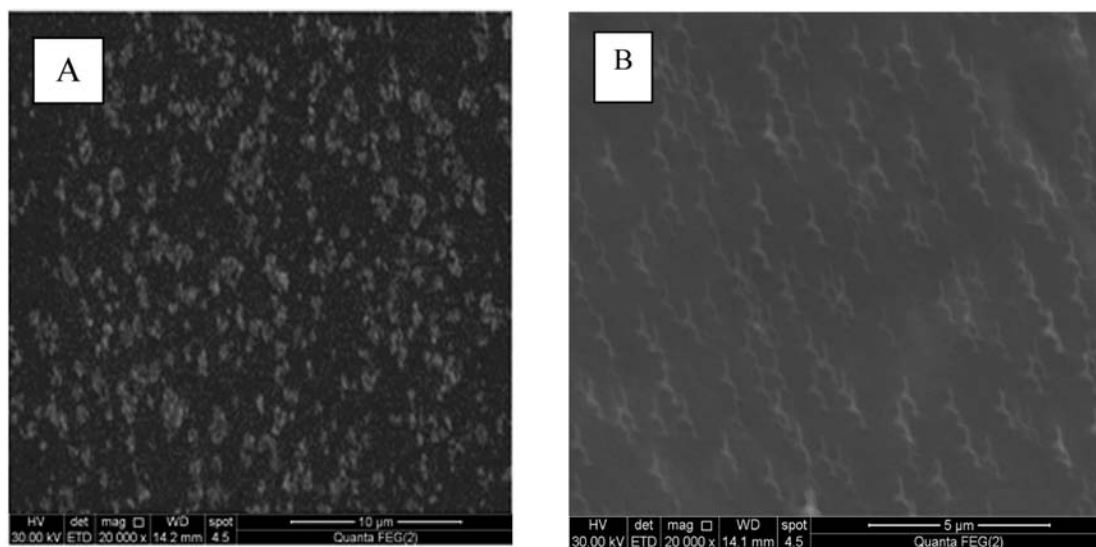


**Fig. 13.** FE-SEM images of GC/NiO<sub>x</sub> (A) and GC<sub>ox</sub>/NiO<sub>x</sub>(B).

and after activation (B) of the surface in 0.1 M of  $H_2SO_4$ . An interesting feature that can be seen in Fig. 13B is that the  $NiO_x$  is bearing a bird-like structure with nanoparticles of uniform size, and ordered shape and direction, with much smaller particle size. Analysis of the SEM images in Fig. 13 obtained from different parts of the samples shows that the predominant particle size of  $NiO_x$  is  $130 \pm 20$  nm and that after oxidative treatment of GC is  $(70 \times 650 \text{ nm}) \pm 10$  nm.

### 2.2.2. Electrochemical characterizations

Table 2 shows the time required for deposition of a fixed amount of Ni on pretreated GC. The latter was pretreated by anodic oxidation at different anodic potentials  $E_{\text{anodic}}$ , for different time periods. The fixed amount of Ni corresponds to a fixed amount of electrodeposition charge  $Q$ , equal to 15 mC in the present case. This amount of charge, assuming 100% coulombic efficiency, corresponds to a loading of Ni equal to  $\sim 0.065 \text{ mg cm}^{-2}$ . The time required for deposition of the same loading of Ni, i.e., the same amount of  $Q$  decreases with the oxidation potential and time periods used in the GC oxidation. The modification of GC with nanoparticles of  $NiO_x$  was performed as discussed earlier in this review. Two GC electrodes were used; glassy carbon without activation (GC) and GC after anodic oxidation at a specific anodic

potential for different time periods ( $GC_{\text{ox}}$ ). Since the rate of electrochemical reaction increases with the increase in the electrode surface area, the time for electrodeposition decreases with the increase in the GC surface area (due to anodic oxidation, see Fig. 12B). This is clearly evident from Table 2. For instance, while 240 s is required to pass 15 mC at the untreated GC electrode, it requires only 95 s to pass the same amount of charge (same amount of the deposited Ni) at the oxidized GC. This was attributed to the larger surface area and higher reactivity of the  $GC_{\text{ox}}$  compared to GC. Note that a 15 mC of charge was chosen in this study since it is enough to obtain a high concentration of  $NiO_x$  and it is not too high with respect to the practical limit since it is reported that higher loadings of  $NiO_x$  than the above value do not increase the activity of  $NiO_x$  [197, 198].

### 2.2.3. Glucose oxidation

Fig. 14 shows CV responses for glucose oxidation on  $GC_{\text{ox}}/NiO_x$  using 20 mM glucose in 0.5 M NaOH. Prior to the electrodeposition of Ni, the GC was oxidized at 1 (D), 1.5 (E) and 2 V (F). The same amount of charge ( $Q = 15$  mC) was used to deposit Ni on GC and  $GC_{\text{ox}}$  electrodes. Curves A and B in Fig. 14 show CV responses for glucose oxidation on GC and  $GC_{\text{ox}}$ , respectively. The peak current for glucose oxidation increases dramatically on the  $GC_{\text{ox}}/NiO_x$  (D-F) compared to

**Table 2.** Time required ( $t_{\text{dep}}$ ) for deposition of fixed amount of Ni ( $Q = 15$  mC in all cases) on GC pre-treated by anodic oxidation at different anodic potential  $E_{\text{anodic}}$ , for different time periods. The table also cites the peak current for glucose oxidation,  $I_p$ . It also shows RSD ( $n = 3$ ) for the peak current.

Time period for anodic oxidation of GC/s	$E_{\text{anodic}}/V$	$t_{\text{dep}}/s$	$I_p/\mu A$	RSD %
0	Untreated	240	314	2.87
60	1	130	411	3.04
	1.5	115	460	2.50
	2	95	490	2.75
120	1	110	455	2.53
	1.5	80	561	2.33
	2	55	622	2.60
300	1	80	492	3.48
	1.5	65	653	3.32
	2	45	735	2.86

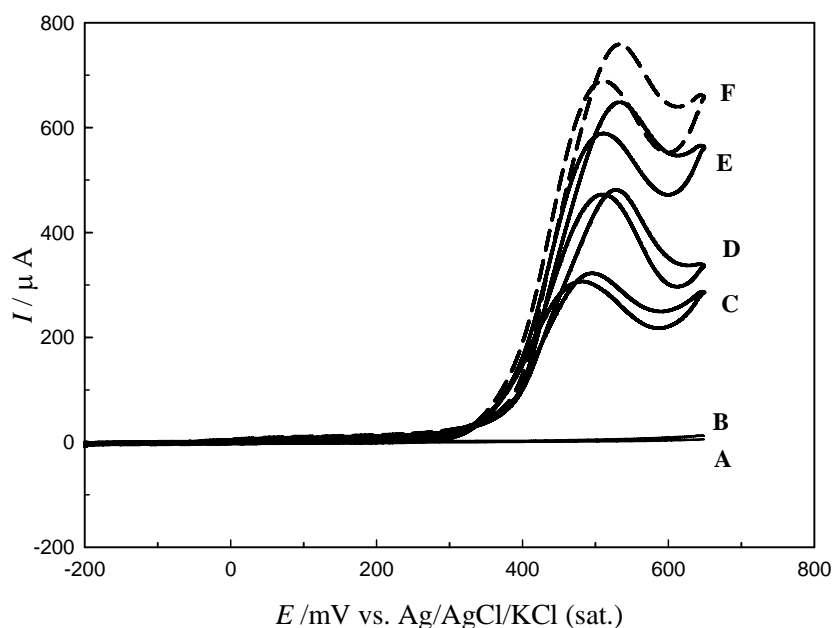


**Fig. 14.** CV responses for glucose oxidation at different electrodes in 0.5 NaOH containing 20 mM of glucose solution using scan rate of  $100 \text{ mV s}^{-1}$ : GC (A),  $\text{GC}_{\text{ox}}$  (B),  $\text{GC}/\text{NiO}_x$  (C) and  $\text{GC}_{\text{ox}}/\text{NiO}_x$  (D-F) where GC was pre-treated by oxidation in 0.1 M of  $\text{H}_2\text{SO}_4$  for 300 s at different anodic potentials: 1.0 V (D), 1.5 V (E), and 2.0 V (F).

that on the  $\text{GC}/\text{NiO}_x$  (C). As the potential used for GC oxidation increases, the peak current for glucose oxidation increases (from curve D to F). The same results were obtained for different time periods of anodic oxidation of GC. As seen from curves A and B in Fig. 14, the GC or  $\text{GC}_{\text{ox}}$  do not have any significant electrocatalytic activity for glucose oxidation and hence  $\text{NiO}_x$  nanoparticles are essential for higher rates of the glucose oxidation.

Note that 15 mC was passed during Ni electrodeposition on both GC and  $\text{GC}_{\text{ox}}$  at all conditions (see Table 2). That is to say, the enhancement in the peak current of glucose oxidation is not attributed to different loadings of  $\text{NiO}_x$  but rather to the modification of the GC surface by anodic oxidation. The reproducibility of the peak current of glucose oxidation  $I_p$  was evaluated by estimating the relative standard deviation (RSD) with ( $n = 3$ , i.e., three replicate measurements) and the values of RSD are given in Table 2. The RSD values ranging from 2.5 to 3.5% are obtained which points to good reproducibility.

It can be concluded that the enhancement is attributable to the increase in the substrate (GC) surface area which gives rise to a better exposure

of the  $\text{NiO}_x$  nanoparticles to glucose oxidation. As evident from the SEM images in Fig. 13, the size of  $\text{NiO}_x$  nanoparticles deposited on  $\text{GC}_{\text{ox}}$  is much lower than that deposited on the untreated GC. The decrease in the size of  $\text{NiO}_x$  nanoparticles is accompanied by an increase in its surface area and hence an increase in the peak current of glucose oxidation. Also, a possible synergism between  $\text{NiO}_x$  and the newly generated C-O functional groups exists. Further possibility is that the preferable deposited phase may be the active  $\beta\text{-NiOOH}$  rather than less active  $\gamma\text{-NiOOH}$ .

It is well documented in literature that anodic oxidation of GC in  $\text{H}_2\text{SO}_4$  results in an increase of the percentage surface composition of C-O functional groups bearing the OH group. For instance, see XPS work performed in [198], and other important work by Jovanovic *et al.*, [195, 196]. The electrocatalytic oxidation of glucose [197, 198] and other small organic molecules such as methanol [197] is enhanced by the presence of the OH group adsorbed on the GC surface (i.e.,  $\text{OH}_{\text{ads}}$ ).

The authors in Ref. [194] showed that the predominant C-O functional groups on glassy carbon (either polished or treated) are phenolic, carboxyl

and carbonyl. XPS examinations of GC oxidized in  $\text{H}_2\text{SO}_4$  showed the enhancement in the fraction of all C-O functional groups; highest increase was in the phenolic and carboxyl groups and lowest increase was in the carbonyl group. Accordingly, the higher percentage of acidic groups on the oxidized GC should promote the higher fraction of oxygen containing species in the  $\text{GC}_{\text{ox}}/\text{NiO}_x$  catalyst than in the  $\text{GC}/\text{NiO}_x$ . Consequently, the  $\text{GC}_{\text{ox}}/\text{NiO}_x$  is more active in glucose oxidation compared to  $\text{GC}/\text{NiO}_x$ .

Another potential role of GC substrate in the higher activity of  $\text{GC}_{\text{ox}}/\text{NiO}_x$  electrodes is that OH-like functional groups on glassy carbon (phenolic, carboxyl) participate in the oxidation of the adsorbed intermediate species formed during glucose dissociation [197, 198]. Increased activity of  $\text{GC}_{\text{ox}}/\text{NiO}_x$  electrode can be attributed to the higher percentage of acidic, i.e., OH-containing groups at oxidized GC surface compared to the polished one. Besides,  $\text{NiO}_x$  of smaller particle size (see Fig. 13), uniformly distributed at oxidized GC have higher number of active sites closely

located to OH-like groups on  $\text{GC}_{\text{ox}}$ . Thus, the effect of OH-like groups participating in the oxidation of the adsorbed intermediates must be much higher and therefore the activity of  $\text{GC}_{\text{ox}}/\text{NiO}_x$  electrode must be remarkably increased for glucose oxidation in comparison with  $\text{GC}/\text{NiO}_x$ .

Further investigation of the enhancement and increase of the sensitivity of  $\text{GC}_{\text{ox}}/\text{NiO}_x$  for glucose oxidation was demonstrated by performing LSV at different glucose concentrations at both  $\text{GC}/\text{NiO}_x$  and  $\text{GC}_{\text{ox}}/\text{NiO}_x$  at the same conditions. These are shown in Fig. 15. Two LSVs corresponding to two concentrations of glucose are only shown for simplicity. The inset shows the relationship between the peak current of glucose oxidation and the glucose concentration at the range of 2-40 mM. The onset potential of glucose oxidation shifts to more negative values at  $\text{GC}_{\text{ox}}/\text{NiO}_x$  and also at higher concentrations of glucose. As the concentration increases, the peak current increases linearly up to  $[\text{glucose}] < 20 \text{ mM}$ . The fact that the rate of glucose oxidation increases with the  $[\text{glucose}]$  indicates that glucose oxidation on both electrodes is a

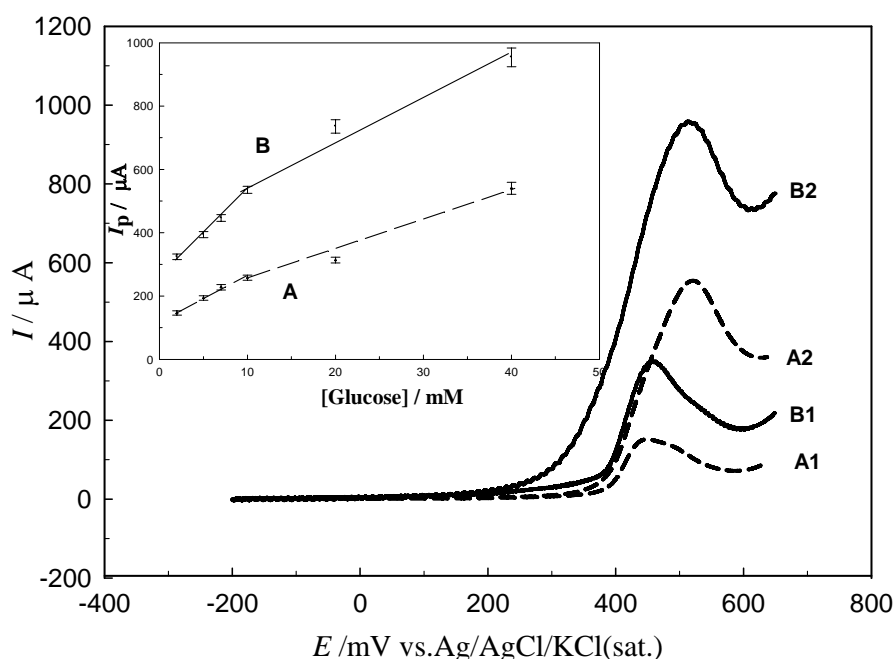


**Fig. 15.** LSV responses for glucose oxidation in 0.5 NaOH containing different glucose concentrations at a scan rate of  $100 \text{ mV s}^{-1}$  at  $\text{GC}/\text{NiO}_x$  (A) and  $\text{GC}_{\text{ox}}/\text{NiO}_x$  (B) electrodes where GC was pre-treated by oxidation at 2 V in 0.1 M of  $\text{H}_2\text{SO}_4$  for 300 s. The digits 1 and 2 refer to  $[\text{glucose}] = 2$  and 40 mM, respectively. The inset shows the relationship between the peak current  $I_p$  and  $[\text{glucose}]$  at  $\text{GC}/\text{NiO}_x$  (A) and at  $\text{GC}_{\text{ox}}/\text{NiO}_x$  (B) electrodes.

typical electrocatalytic response. It can be suggested that the above relation between  $I_p$  and [glucose] is due to a diffusion-controlled process. Thus, diffusion plays an important role at the concentration range < 20 mM.

### 3. Conclusion

In this article, we reviewed the different aspects of electrocatalytic oxidation of glucose. One main purpose was to focus on the general outline of the electrocatalytic oxidation of glucose and its potential use as a half-reaction in direct glucose fuel cell or biochemical fuel cells. On the other hand, a potential use of such reaction is in biosensor and determination of glucose concentration in blood and in food industry. Our previous work was also reviewed here.

A novel binary catalyst of nickel and manganese oxide, with considerable stability, was electrochemically fabricated on the GCE in a specific order. It was found that electrochemical activity for glucose oxidation depends critically on the loading level and order of electrodeposition of the two catalysts. Under the present conditions, it has been found that the optimum loading level is 60 cycles of  $MnO_y$  followed by 10 min. of nickel deposition. At this loading level, the relationship between the  $I_p/v^{1/2}$  function and scan rate confirm the fact that glucose reaction is a catalytic process. The rate-determining step was found to be the one electron transfer process, which demonstrates the catalytic role of nickel hydroxide.

Halide ions have significant poisoning effect on the electrocatalytic activity of  $NiO_x/MnO_y/GC$  electrode for glucose oxidation in alkaline medium. The poisoning degree of halide ions depends largely on their chemical structure and concentration in solution. Our fabricated electrode has high tolerance towards chloride and bromide ions even at high concentrations up to 0.3 M. While for iodide ion, it was found that, it has a significant effect on glucose oxidation in our operating conditions at concentrations much lower in comparison with that of the other two halide ions. The  $NiO_x/MnO_y/GC$  can be considered as a good catalyst for glucose oxidation even in the presence of a large concentration of  $Cl^-$ .

The anodic oxidation of GC in 0.1 M  $H_2SO_4$  has significant effects on the electrodeposition of Ni

on GC and subsequently on the catalytic oxidation of glucose from alkaline solutions. The effects of the potential and time period used in the anodic oxidation of GC on the glucose oxidation were studied. The shape and size of  $NiO_x$  nanoparticles electrodeposited on  $GC_{ox}$  is different than those electrodeposited on GC. The pretreatment of GC by anodic oxidation has its impact on the redox couple of  $NiO_x$ , i.e., on the  $Ni(OH)_2 \leftrightarrow NiOOH$ . This was attributed to the increase in the GC surface area and to the concentration of C-O functional groups. The peak current of glucose oxidation is increased at  $GC_{ox}/NiO_x$  compared to  $GC/NiO_x$  which is an indication of the enhanced glucose oxidation at the former electrode.

### CONFLICT OF INTEREST STATEMENT

The authors declare that there are no conflicts of interest.

### REFERENCES

1. Bankar, S. B., Bule, M. V., Singhal, R. S. and Ananthanarayan, L. 2009, *Biotechnol. Advances*, 27, 489.
2. Quan, H., Park, S. and Park, J. 2010, *Electrochim. Acta*, 55, 2232.
3. Newman, J. D. and Turner, A. P. F. 2005, *Biosens. Bioelectron.*, 20, 2435.
4. Wilson, G. S. and Gifford, R. 2005, *Biosens. Bioelectron.*, 20, 2388.
5. Ramanavicius, S. Kausaite, A. and Ramanaviciene, A. 2005, *Biosens. Bioelectron.*, 20, 1962.
6. Updike, S. and Hicks, G. 1967, *Nature*, 214, 986.
7. Wang, J. and Pamidi, P. V. A. 1997, *Anal. Chem.*, 69, 4490.
8. Patolsky, F., Weizmann, F., Y. and Willner, Y. I. 2004, *Angew. Chem.*, 43, 2113.
9. Wang, J. 2008, *Chem. Rev.*, 108, 814.
10. Park, S., Boo, H. and Chung, T. D. 2006, *Anal. Chim. Acta*, 556, 46.
11. Clark, L. C. and Lyons, J. C. 1962, *Ann. N. Y. Acad. Sci.*, 102, 29.
12. Zhang, Y. W., Chang, G. H., Liu, S., Lu, W. B., Tian, J. Q. and Sun, X. P. 2011, *Biosens. Bioelectron.*, 28, 344.
13. Shinohara, H., Chiba, T. and Aizawa, M. 1988, *Sens. Actuators*, 13, 79.

14. Kajiya, Y., Sugai, H., Iwakura, C. and Yoneyama, H. 1991, *Anal. Chem.*, 63, 49.
15. Fabiano, S., Tran-Minh, C., Piro, B., Dang, L. A., Pham, M. C. and Vittori, O. 2002, *Mater. Sci. Eng.*, C21, 61.
16. Gao, M., Dai, L. and Wallace, G. G. 2003, *Synth. Metals*, 137, 1393.
17. Pan, D., Chen, J., Yao, S., Tao, W. and Nie, L. 2005, *Anal. Sci.*, 21, 367.
18. Ramanathan, K., Pandey, S. S., Kumar, R., Gulati, A., Murthy, A. S. N. and Malhotra, B. D. 2000, *J. Appl. Polym. Sci.*, 78, 7.
19. Rahman, M. A., Park, D. S. and Shim, Y. B. 2004, *Biosens. Bioelectron.*, 19, 1565.
20. Rajesh Bisht, V., Takashima, W. and Kaneto, K. 2005, *Surf. Coat. Technol.*, 198, 231.
21. Kuwahara, T., Homma, T., Kondo, M. and Shimomura, M. 2009, *Synth. Metals*, 159, 1859.
22. Senel, M. and Nergiz, C. 2012, *Curr. Appl. Phys.*, 12, 1118.
23. Jiang, H., Zhang, A., Sun, Y., Ru, X., Ge, D. and Shi, W. 2012, *Electrochim. Acta*, 70, 278.
24. Chen, T., Friedman, K. A., Lei, I. and Heller, A. 2002, *Anal. Chem.*, 72, 3757.
25. Guo, G. M., Chen, Q. A. and Chen, X. 2011, *Sci. China Chem.*, 54, 1777.
26. Guo, G. M., Wang, X. D., Zhou, T. Y. and Chen, X. 2010, *Sci. China Chem.*, 53, 1385.
27. Kausaite-Minkstimiene, A., Mazeiko, V., Ramanaviciene, A. and Ramanavicius, A. 2010, *Biosens. Bioelectron.*, 26, 790.
28. Cosnier, S. 1999, *Biosens. Bioelectron.*, 14, 443.
29. Heller, J. and Heller, A. 1998, *J. Am. Chem. Soc.*, 120, 4586.
30. Ratner, B. D. 1995, *Biosens. Bioelectron.*, 10, 797.
31. Chaudhury, M. K. 1995, *Biosens. Bioelectron.*, 10, 785.
32. Gooding, J. J. and Hibbert, D. B. 1999, *Trends Anal. Chem.*, 18, 525.
33. Willner, I., Katz, E. and Willner, B. 1997, *Electroanalysis*, 9, 965.
34. Frretti, S., Paynter, S., Russell, D. A., Sapsford, K. E. and Richardson, D. J. 2000, *Trends Anal. Chem.*, 19, 530.
35. Toghiani, K. E. and Compton, R. G. 2010, *Int. J. Electrochem. Sci.*, 5, 1246.
36. Hu, Y., Song, Y., Wang, Y. and Di, J. 2011, *Thin Solid Films*, 519, 6605.
37. Atta, N. F., Galal, A. and El-Ads, E. H. 2012, *Electrochim. Acta*, 69, 102.
38. Tominaga, M., Shimazoe, T., Nagashima, M., Kusuda, H., Kubo, A., Kuwahara, Y. and Taniguchi, I. 2006, *J. Electroanal. Chem.*, 590, 37.
39. Cho, S., Shin, H. and Kang, C. 2006, *Electrochim. Acta*, 51, 3781.
40. Seo, B., Choi, S. and Kim, J. 2011, *ACS Applied Mater. and Interf.*, 3, 441.
41. Pasta, M., Mantia, Fabio, L. and Cui, Y. 2010, *Electrochem. Commun.*, 12, 1407.
42. Habrioux, A., Servat, K., Girardeau, T., Guérin, P., Napporn, T. W. and Kokoh, K. B. 2011, *Curr. Appl. Phys.*, 11, 1149.
43. Mazeiko, V., Kausaite-Minkstimiene, A., Ramanaviciene, A., Balevicius, Z. and Ramanavicius, A. 2011, *Sens. Actuators B: Chem.*, 152, 37.
44. Jeong, H. and Kim, J. 2012, *Electrochim. Acta*, 80, 383.
45. Liu, A., Ren, Q., Xu, T., Yuan, M. and Tang, W. 2012, *Sens. Actuators B: Chem.*, 162, 135.
46. Wang, Q., Min, F. and Zhu, F. 2013, *Mater. Lett.*, 91, 9.
47. Li, Y., Song, Y. Y., Yang, C. and Xia, X. H. 2007, *Electrochem. Commun.*, 9, 981.
48. Cho, S. and Kang, C. 2007, *Electroanalysis*, 19, 2315.
49. Bai, Y., Yang, W. W., Sun, Y. and Sun, C. Q. 2008, *Sens. and Actuators B: Chem.*, 134, 471.
50. Xia, Y., Huang, W., Zheng, J. F., Niu, Z. J. and Li, Z. L. 2011, *Biosens. and Bioelectron.*, 26, 3555.
51. Hyun, M., Choi, S. and Kim, J. 2010, *Anal. Sci.*, 26, 129.
52. Liu, Z., Du, J., Qiu, C., Huang, L., Ma, H., Shen, D. and Ding, Y. 2009, *Electrochem. Commun.*, 11, 1365.
53. Seo, B. and Kim, J. 2010, *Electroanalysis*, 22, 939.
54. Deng, Y. P., Huang, W., Chen, X. and Li, Z. L. 2008, *Electrochem. Commun.*, 10, 810.
55. Nishio, K. and Masuda, H. 2011, *Angew. Chem. Int. Ed.*, 50, 1603.

56. Zhao, W., Xu, J. J., Shi, C. G. and Chen, H. Y. 2006, *Electrochem. Commun.*, 8, 773.
57. Zhou, Y. G., Yang, S., Qian, Q. Y. and Xia, X. H. 2009, *Electrochem. Commun.*, 11, 216.
58. Qiu, H. J. and Huang, X. R. 2010, *J. Electroanal. Chem.*, 643, 39.
59. Tavakkoli, N. and Nasrollahi, S. 2013, *Aust. J. Chem.*, 66, 1097.
60. Bai, H. Y., Han, M., Du, Y. Z., Bao, J. and Zhihui, D. 2010, *Chem. Commun.*, 46, 1739.
61. Chen, X. M., Cai, Z. M., Lin, Z. J., Jia, T. T., Liu, H. Z., Jiang, Y. Q. and Chen, X. 2009, *Biosens. Bioelectron.*, 24, 3475.
62. Meng, L., Jin, J., Yang, G., Lu, T., Zhang, H. and Cai, C. 2009, *Anal. Chem.*, 81, 7271.
63. Zhang, W. J., Baia, L., Lua, L. M. and Chen, Z. 2012, *Colloids Surf. B: Biointerf.*, 97, 145.
64. Gutés, A., Carraro, C. and Maboudian, R. 2011, *Electrochim. Acta*, 56, 5855.
65. Lu, L. M., Li, H. B., Qub, F., Zhang, X. B., Shen, G. L. and Yu, R. Q. 2011, *Biosens. Bioelectron.*, 26, 3500.
66. Szunerits, S. and Boukherroub, R. 2008, *Comp. Rend. Chim.*, 1, 1004.
67. Atta, N. F. and El-Kady, M. F. 2009, *Talanta*, 79, 639.
68. Liao, F., Wang, Z., Guo, T., Zhang, T. and Wu, Z. 2012, *J. Electroanal. Chem.*, 673, 38.
69. Santhosh, P., Manesh, K. M., Uthayakumar, S., Komathi, S., Gopalan, K. P. and Lee, A. I. 2009, *Bioelectrochem.*, 75, 61.
70. Reyter, D., Odziemkowski, M., Bélanger, D. and Roué, L. 2007, *J. Electrochem. Soc.*, 154, K36.
71. Zhao, J., Wei, L. M., Peng, C. H., Su, Y. J., Yang, Z., Zhang, L. Y., Wei, H. and Zhang, Y. F. 2013, *Biosens. and Bioelectron.*, 47, 86.
72. Zhao, Y., Zhao, J. Z., Ma, D. C., Li, Y. L., Hao, X. L., Li, L. Z., Yu, C. Z., Zhang, L., Lu, Y. and Wang, Z. C. 2012, *Colloids and Surf.*, A409, 105.
73. Jiang, L.-C. and Zhang, W.-D. 2010, *Biosens. and Bioelectron.*, 25, 1402.
74. Wu, H. X., Cao, W. M., Li, Y., Liu, G., Wen, Y., Yang, H. F. and Yang, S-P. 2010, *Electrochim. Acta*, 55, 3734.
75. Yang, J. A., Zhang, W. D. and Gunasekaran, S. 2010, *Biosens. and Bioelectron.*, 26, 279.
76. Jiang, F., Wang, S., Lin, J. J., Jin, H. L., Zhang, L. J., Huang, S. M. and Wang, J. 2001, *Electrochem. Commun.*, 13, 363.
77. Lu, L. M., Zhang, X. B., Shen, G. L. and Yu, R. Q. 2012, *Anal. Chim. Acta*, 715, 99.
78. Yang, Z. Y., Feng, J. S., Qiao, J. S., Yan, Y. M., Yu, Q. Y. and Sun, K. N. 2012, *Anal. Methods*, 4, 1924.
79. Zhou, X. M., Nie, H. G., Yao, Z., Dong, Y. Q., Yang, Z. and Huang, S. M. 2012, *Sens. and Actuators B: Chem.*, 168, 1.
80. Yang, G. C., Liu, E. J., Khun, N. W. and Jiang, S. P. 2009, *J. Electroanal. Chem.*, 627, 51.
81. Nie, H. G., Yao, Z., Zhou, X. M., Yang, Y. and Huang, S. M. 2011, *Biosens. Bioelectron.*, 30, 28.
82. You, T., Niwa, O., Chen, Z., Hayashi, K., Tomita, M. and Hirono, S. 2003, *Anal. Chem.*, 75, 5191.
83. Mu, Y., Jia, D. L., He, Y. Y., Miao, Y. Q. and Wu, H. L. 2011, *Biosens. Bioelectron.* 26, 2948.
84. Safavi, A., Maleki, N. and Farjami, E. 2009, *Biosens. Bioelectron.*, 24, 1655.
85. de Mele, M. F. L., Videla, H. A. and Arvía, A. J. 1983, *Bioelectrochem. Bioenerg.*, 10, 239.
86. Park, S., Chung, D. T. and Kim, H. C. 2003, *Anal. Chem.*, 75, 3046.
87. Yuan, J. H., Wang, K. and Xia, X. H. 2005, *Adv. Funct. Mater.*, 15, 803.
88. Guo, M., Fang, H., Hong, H., Tang, N. and Xu, X. 2012, *Electrochim. Acta*, 63, 1.
89. Wang, J., Thomas, D. F. and Chen, A. 2008, *Anal. Chem.*, 80, 997.
90. Song, Y. Y., Zhang, D., Gao, W. and Xia, X. H. 2005, *Chem. Eur. J.*, 11, 2177.
91. Shen, Q. M., Jiang, L. P., Zhang, H., Min, Q. H., Hou, W. H. and Zhu, J. J. 2008, *J. Phys. Chem. C*, 11, 16385.
92. Ryu, J., Kim, K., Kim, H., Hahn, H. T. and Lashmore, D. 2010, *Biosens. Bioelectron.*, 26, 602.
93. Safavi, A. and Farjami, F. 2011, *Biosens. Bioelectron.*, 26, 2547.
94. Bai, Y., Sun, Y. and Sun, C. 2008, *Biosens. Bioelectron.*, 24, 579.
95. Bo, X., Bai, J., Qi, B. and Guo, L. 2011, *Biosens. Bioelectron.*, 28, 77.

96. Ding, Y., Liu, Y., Parisi, J., Zhang, L. and Lei, Y. 2011, *Biosens. Bioelectron.*, 28, 393.
97. Li, L.-H., Zhang, W.-D. and Ye, J.-S. 2008, *Electroanalysis*, 20, 2212.
98. Xiao, F., Li, Y., Gao, H., Ge, S. and Duan, H. 2013, *Biosens. Bioelectron.*, 41, 417.
99. Liu, Y., Ding, Y., Zhang, Y. and Lei, Y. 2012, *Sens. Actuators B*, 171-172, 954.
100. Chen, J., Wiley, B., McLellan, J., Xiong, Y., Li, Z. Y. and Xia, Y. N. 2005, *Nano Lett.*, 5, 2058.
101. Guo, S. J., Dong, S. J. and Wang, E. K. 2010, *Chem. Commun.*, 46, 1869.
102. Basu, D. and Basu, S. 2011, *Electrochim. Acta*, 56, 6106.
103. Basu, D. and Basu, S. 2010, *Electrochim. Acta*, 55, 5775.
104. Liu, Z., Huang, L., Zhang, L., Ma, H. and Ding, Y. 2009, *Electrochim. Acta*, 54, 7286.
105. Jin, C. and Taniguchi, I. 2007, *Mater. Lett.*, 61, 2365.
106. Cuevas-Muniz, F. M., Guerra-Balcázar, M., Castaneda, F., Ledesma-García, J. and Arriaga, L. G. 2011, *J. Power Sourc.*, 196, 5853.
107. Zhu, C., Guo, S. and Dong, S. 2012, *Adv. Mater.*, 24, 2326.
108. Cui, H. F., Ye, J. S., Liu, X., Zhang, W. D. and Sheu, F. S. 2006, *Nanotechnology*, 17, 2334.
109. Sun, Y., Buck, H. and Mallouk, T. E. 2001, *Anal. Chem.*, 73, 1599.
110. Cao, X., Wang, N., Jia, S. and Shao, Y. H. 2013, 85, 5040.
111. Tonda-Mikiela, P., Napporn, T. W., Morais, C., Servat, K., Chen, A. and Kokoh, K. B. 2012, *J. Electrochem. Soc.*, 159, H828.
112. Gao, H. C., Xiao, F., Ching, C. B. and Duan, H. W. 2011, *ACS Appl. Mater. Interface*, 3, 3049.
113. Hermans, S., Deffernez, A. and Devillers, M. 2011, *Appl. Catal. A: Gen.*, 395, 19.
114. Li, C., Liu, Y., Li, L., Du, Z., Xu, S., Zhang, M., Yin, X. and Wang, T. 2008, *Talanta*, 77, 455.
115. Xia, C. and Ning, W. 2010, *Electrochem. Commun.*, 12, 1581.
116. Das, D., Sen, P. and Das, K. 2006, *J. Appl. Electrochem.*, 36, 685.
117. Shim, J., Kang, M., Lee, Y. and Lee, C. 2012, *Microchim. Acta*, 177, 211.
118. Zhang, L., Li, H., Ni, Y., Li, J., Liao, K. and Zhao, G. 2009, *Electrochem. Commun.*, 11, 812.
119. Ding, Y., Wang, Y., Su, L., Bellagamba, M., Zhang, H. and Lei, Y. 2010, *Biosens. and Bioelectron.*, 26, 542.
120. Bai, Y., Sun, Y. and Sun, C. 2008, *Biosens. Bioelectron.*, 24, 579.
121. Lei, Y., Yan, X., Zhao, J., Liu, X., Song, Y., Luo, N. and Zhang, Y. 2011, *Colloids and Surf. B: Biointerf.*, 82, 168.
122. Berchmans, S., Gomathi, H. and Rao, G. P. 1995, *J. Electroanal. Chem.*, 394, 267.
123. Lyons, M. E. G., Fitzgerald, C. A. and Smyth, M. R. 1994, *Analyst*, 119, 855.
124. Chen, J. W., Zhang, D. and Ye, J. S. 2008, *Electrochem. Commun.*, 10, 1268.
125. Noorbakhsh, A. and Salimi, A. 2009, *Electrochim. Acta*, 54, 6312.
126. Nam, K. W. and Kim, K. B. 2002, *J. Electrochem. Soc.*, 149, A346.
127. Zhang, Y., Xu, F. G., Sun, Y. J., Shi, Y., Wen, Z. W. and Li, Z. 2011, *J. Mater. Chem.*, 21, 16949.
128. Li, X., Liu, J. P., Ji, X. X., Jiang, J., Ding, R. M., Hu, Y. Y., Hu, A. Z. and Huang, X. T. 2010, *Sens. Actuators B: Chem.*, 147, 241.
129. Zhang, Y. C., Su, L., Manuzzi, D., Jia, W. J., Huo, D. Q., Hou, C. J. and Lei, Y. 2012, *Biosens. Bioelectron.*, 31, 426.
130. Li, S., Zheng, Y. J., Qin, G. W., Ren, Y. P., Pei, W. L. and Zuo, L. 2011, *Talanta*, 85, 1260.
131. Cherevko, S. and Chung, C. H. 2010, *Talanta*, 80, 1371.
132. Tong, S. F., Jin, H. Y., Zheng, D. F., Wang, W., Li, X., Xu, Y. H. and Song, W. B. 2009, *Biosens. Bioelectron.*, 24, 2404.
133. Luo, J., Jiang, S. S., Zhang, H. Y., Jiang, J. Q. and Liu, X. Y. 2012, *Anal. Chim. Acta*, 709, 47.
134. Li, X., Zhu, Q. Y., Tong, S. F., Wang, W. and Song, W. B. 2009, *Sens. and Actuators B: Chem.*, 136, 444.
135. Luque, G. L., Rodríguez, M. C. and Rivas, G. A. 2005, *Talanta*, 15, 467.

136. Tong, S. F., Xu, Y. H., Zhang, Z. X. and Song, W. B. 2010, *J. Phys. Chem. C*, 114, 20925.
137. Luo, P. F., Prabhu, S. V. and Baldwin, R. P. 1990, *Anal. Chem.*, 62, 752.
138. Luo, P. F. and Kuwana, T. 1994, *Anal. Chem.*, 66, 2775.
139. Casella, I. G., Desimoni, E. and Cataldi, T. R. I. 1991, *Anal. Chim. Acta*, 248, 117.
140. Lu, B. P., Jing, B., Bo, X. J., Zhu, L. D. and Guo, L. P. 2010, *Electrochim. Acta*, 55, 8724.
141. Khatib, K. M. E. and Hameed, R. M. A. 2011, *Biosens. and Bioelectron.*, 26, 3542.
142. Wang, W., Zhang, L. L., Tong, S. F., Li, X. and Song, W. B. 2009, *Biosens. Bioelectron.*, 25, 708.
143. Zhang, X. J., Wang, G. F., Liu, X. W., Wu, J. J., Li, M., Gu, J., Liu, H. and Fang, B. 2008, *J. Phys. Chem. A*, 112, 16845.
144. Wang, X., Hu, C. G., Liu, H., Du, G. J., He, X. S. and Xi, Y. 2010, *Sens. Actuators B: Chem.*, 144, 220.
145. Li, C. L., Su, Y., Zhang, S. W., Lv, X. Y., Xia, H. L. and Wang, Y. J. 2010, *Biosens. Bioelectron.*, 26, 903.
146. Zhuang, Z. J., Su, X. D., Yuan, H. Y., Sun, Q., Xiao, D. and Choi, M. F. 2008, *Analyst*, 133, 126.
147. Li, J. Y., Xiong, S. L., Pan, J. and Qian, Y. T. 2010, *J. Phys. Chem. C*, 114, 9645.
148. Reitz, E., Jia, W. Z., Gentile, M., Wang, Y. and Lei, Y. 2008, *Electroanalysis*, 20, 2482.
149. Fleischmann, M., Korinek, K. and Pletcher, D. 1971, *J. Electroanal. Chem.*, 31, 39.
150. Vertes, G. and Horanyi, G. 1974, *J. Electroanal. Chem.*, 52, 47.
151. Robertson, P. M. 1980, *J. Electroanal. Chem.*, 111, 97.
152. Wolf, J. F., Yeh, L.-S. R. and Damjanovic, A. 1981, *Electrochim. Acta*, 26, 4.
153. El-Refaei, S. M., Saleh, M. M. and Awad, M. I. 2014, *J. Solid State Electrochem.*, 18, 5.
154. El-Refaei, S. M., Saleh, M. M. and Awad, M. I. 2013, *J. Power Sourc.*, 223, 125.
155. El-Refaei, S. M., Awad, M. I., El-Anadouli, B. E. and Saleh, M. M. 2013, *Electrochim. Acta*, 92, 460.
156. Ghonim, A. M., El-Anadouli, B. E., Saleh, M. M. 2013, *Electrochim. Acta*, 114, 713.
157. Ghonim, A. M., El-Anadouli, B. E., Saleh, M. M. 2015, *Int. J. Electrochem. Sci.*, 10, in press.
158. Thiagarajan, S., Tsai, T. H. and Chen, S.-M. 2011, *Int. J. Electrochem. Science*, 6, 2235.
159. El-Deab, M. S. 2012, *J. Advanced Res.*, 3, 65.
160. Bode, H., Dehmelt, K. and Witte, J. 1966, *Electrochim. Acta*, 11, 1079.
161. Schreiber Guzmán, R. S., Vilche, J. R. and Arvía, A. J. 1978, *J. Electrochem. Soc.*, 125, 1578.
162. Chen, J., Bradhurst, D. H., Dou, S. X. and Liu, H. K. 1999, *J. Electrochem. Soc.*, 146, 3606.
163. Das, D., Sen, P. K. and Das, K. 2008, *Electrochim. Acta*, 54, 289.
164. Fleischmann, M., Korinek, K. and Pletcher, D. 1972, *J. Chemical Soc., Perkin Trans.*, 2, 1396.
165. Singh, D. 1998, *J. Electrochem. Soc.*, 145, 116.
166. Taraszewska, J. and Rosłonek, G. 1994, *J. Electroanal. Chem.*, 364, 209.
167. Allen, J. R., Florido, A., Young, S. D., Daunert, S. and Bachas, L. G. 1995, *Electroanalysis*, 7, 710.
168. Zhao, C., Shao, C., Li, M. and Jiao, K. 2007, *Talanta*, 71, 1769.
169. Becerik, I. and Kadirgan, F. 1992, *Electrochim. Acta*, 37, 2651.
170. Tominaga, M., Shimazoe, T., Nagashima, M. and Taniguchi, I. 2005, *Electrochem. Comm.*, 7, 189.
171. Mho, S.-I. and Johnson, D. C. 2001, *J. Electroanal. Chem.*, 500, 524.
172. El-Deab, M. S. 2010, *J. Advanced Res.*, 1, 87.
173. Liu, Y., Teng, H., Hou, H. and You, T. 2009, *Biosens. and Bioelectron.*, 24, 3329.
174. Khamis, A., Saleh, M. M. and Awad, M. I. 2013, *Corr. Sci.*, 66, 343.
175. Novak, D. M. and Conway, B. 1981, *J. Chem. Soc., Faraday Trans.*, 77, 2341.
176. Lee, K. K., Loh, P. Y., Sow, C. H. and Chin, W. S. 2012, *Electrochem. Comm.*, 20, 128.
177. Rezwani Miah, Md. and Ohsaka, T. 2006, *Anal. Chem.*, 78, 1200.

- 
178. Anson, F. C. and Lingane, J. J. 1957, *J. Amer. Chem. Soc.*, 75, 1015.
179. Garcia-Miquel, J. L., Zhang, Q., Allen, S. J., Rougier, A., Blyr, A., Davies, H. O., Jones, A. C., Leedham, T. J., William, P. A. and Impey, S. A. 2003, *Thin Solid Films*, 424, 165.
180. Danaee, I., Jafarian, M., Forouzandeh, F., Gobal, F. and Mahjani, M. G. 2008, *Electrochim. Acta*, 53, 6602.
181. Luo, Z., Yin, S., Wang, K., Li, H., Wang, L., Xu, H. and Xia, J. 2012, *Mat. Chem. Phys.*, 132, 387.
182. Engstrom, R. C. 1982, *Anal. Chem.*, 54, 2310.
183. Engstrom, R. D. and Strasser, V. A. 1984, *Anal. Chem.*, 56, 136.
184. Hu, I. F., Karweik, D. H. and Kuwana, T. 1985, *J. Electroanal. Chem.*, 188, 59.
185. Bowling, R. J., Packard, R. T. and McCreery, R. L. 1989, *J. Am. Chem. Soc.*, 111, 1217.
186. Poon, M. and McCreery, R. L. 1986, *Anal. Chem.*, 58, 2745.
187. Poon, M. and McCreery, R. L. 1988, *Anal. Chem.*, 60, 605.
188. Fagan, D. T., Hu, I. F. and Kuwana, T. 1985, *Anal. Chem. J.*, 57, 2759.
189. Zhang, H. and Coury Jr., L. A. 1993, *Anal. Chem.*, 65, 1552.
190. Kovach, P. M., Deakin, M. R. and Wightman, R. M. 1986, *J. Phys. Chem.*, 90, 4612.
191. Cabaniss, G. E., Diamantis, A. A., Murphy, W. R., Linton, R. W. and Meyer, T. J. 1985, *J. Am. Chem. Soc.*, 107, 1845.
192. Zhao, Q.-L., Zhang, Z.-L., Bao, L. and Pang, D.-W. 2008, *Electrochem. Comm.*, 10, 181.
193. Jovanovic, V. M., Terzic, S., Tripkovic, A. V., Popovic, K. D. and Lov, J. D. 2004, *Electrochem. Comm.*, 6, 1254.
194. Jovanovic, V. M., Tripkovic, D., Tripkovic, A. and Kowal, A. 2005, *J. Stoch. Electrochem. Comm.*, 7, 1039.
195. Stevanovic, S., Panic, V., Tripkovic, D. and Jovanovic, V. M. 2009, *Electrochem. Comm.*, 11, 18.
196. Saleh, M. M., Awad, M. I., Okajima, T., Suga, K. and Ohsaka, T. 2007, *Electrochim. Acta*, 52, 3095.
197. Vassilyev, Y. B., Khazova, O. A. and Nikolaeva, N. N. 1985, *J. Electroanal. Chem.*, 196, 127.
198. Hsiao, M. W., Adzic, R. R. and Yeager, E. B. 1992, *Electrochimica Acta*, 37, 357.